NUREG/CR–4744
Vol. 4, No. 1
ANL–90/44

Long-Term Embrittlement of Cast Duplex Stainless Steels in LWR Systems

Semiannual Report
October 1988–March 1989

Prepared by O. K. Chopra, H. M. Chung

Argonne National Laboratory

Prepared for
U.S. Nuclear Regulatory Commission

NUREG/CR--4744-Vol.4-No.1

TI91 012497

Long-Term Embrittlement of Cast Duplex Stainless Steels in LWR Systems

Semiannual Report
October 1988–March 1989

Manuscript Completed: November 1990
Date Published: May 1991

Prepared by
O. K. Chopra, H. M. Chung

Argonne National Laboratory
9700 South Cass Avenue
Argonne, IL 60439

Prepared for
Division of Engineering
Office of Nuclear Regulatory Research
U.S. Nuclear Regulatory Commission
Washington, DC 20555
NRC FIN A2243

Previous Documents in Series

Long-Term Embrittlement of Cast Duplex Stainless Steels in LWR Systems: Annual Report October 1982–September 1983, NUREG/CR–3857, ANL–84–44 (August 1984).

Long-Term Embrittlement of Cast Duplex Stainless Steels in LWR Systems: Annual Report October 1983–September 1984, NUREG/CR–4204, ANL–85–20 (March 1985).

Long-Term Embrittlement of Cast Duplex Stainless Steels in LWR Systems: Annual Report October 1984–September 1985, NUREG/CR–4503, ANL–86–3 (January 1986).

Long-Term Embrittlement of Cast Duplex Stainless Steels in LWR Systems: Semiannual Report October 1985–March 1986, NUREG/CR–4744 Vol. I, No. 1, ANL–86–54 (September 1986).

Long-Term Embrittlement of Cast Duplex Stainless Steels in LWR Systems: Semiannual Report April–September 1986, NUREG/CR–4744 Vol. I, No. 2, ANL–87–16 (March 1987).

Long-Term Embrittlement of Cast Duplex Stainless Steels in LWR Systems: Semiannual Report October 1986–March 1987, NUREG/CR–4744, Vol. 2, No. 1, ANL–87–45 (July 1987).

Long-Term Embrittlement of Cast Duplex Stainless Steels in LWR Systems: Semiannual Report April–September 1987, NUREG/CR–4744, Vol. 2, No. 2, ANL–89/6 (July 1989).

Long-Term Embrittlement of Cast Duplex Stainless Steels in LWR Systems: Semiannual Report October 1987–March 1988, NUREG/CR–4744, Vol. 3, No. 1, ANL–89/22 (February 1990).

Long-Term Embrittlement of Cast Duplex Stainless Steels in LWR Systems: Semiannual Report April–September 1988, NUREG/CR–4744, Vol. 3, No. 2, ANL–90/5 (August 1990).

Long–Term Embrittlement of Cast Duplex Stainless Steels in LWR Systems

by

O. K. Chopra and H. M. Chung

Abstract

This progress report summarizes work performed by Argonne National Laboratory on long–term embrittlement of cast duplex stainless steels in LWR systems during the six months from October 1988 to March 1989. Charpy–impact data are presented for several heats of cast stainless steel aged at temperatures between 320 and 450°C for times up to 30,000 h. Thermal aging decreases impact energy and shifts transition curves to higher temperatures. A saturation effect is observed for room–temperature impact energy and upper–shelf energy. Charpy data are analyzed to obtain the activation energy of the kinetics of embrittlement. The results suggest that the activation energy of embrittlement is not constant in the temperature range of 290–400°C, but increases as temperature decreases. A correlation is presented for estimating the extent of embrittlement of cast stainless steels from known material parameters. The degradation in mechanical properties can be reversed by annealing the embrittled material for 1 h at 550°C and then water quenching.

Contents

Figures

Tables

Executive Summary

Cast stainless steels used in pump casings, valve bodies, piping, and other components in coolant systems of light-water nuclear reactors (LWRs) suffer loss of toughness after many years of service at 290–320°C. A program is being conducted to investigate the low-temperature embrittlement of cast duplex stainless steels under LWR operating conditions and to evaluate possible remedies for embrittlement problems in existing and future plants. The scope of the investigation includes the following goals: (1) characterize and correlate the microstructure of in-service reactor components and laboratory-aged material with loss of fracture toughness to establish the mechanism of aging and validate the simulation of in-reactor degradation by accelerated aging, (2) establish the effects of key compositional and metallurgical variables on the kinetics and extent of embrittlement, and (3) develop the methodology and correlations for predicting the toughness loss suffered by cast stainless steel components during normal and extended life of LWRs.

Microstructural and mechanical-property data are being obtained on 25 experimental heats (19 in the form of static-cast keel blocks and 6 in the form of slabs) and 6 commercial heats (centrifugally cast pipes and a static-cast pump impeller and pump casing ring), as well as on reactor-aged material of grades CF-3, CF-8, and CF-8M cast stainless steel. The ferrite content of the cast materials ranges from 3 to 30%. Ferrite morphology for the castings containing >5% ferrite is either lacy or acicular.

Charpy-impact, tensile, and J-R curve tests have been conducted on several experimental and commercial heats of cast stainless steel that were aged up to 30,000 h at 290–400°C. Results indicate that thermal aging at these temperatures increases the tensile strength and decreases the impact energy and fracture toughness of the steels. The Charpy transition curve shifts to higher temperatures. Different heats exhibit different degrees of embrittlement. In general, the low-carbon CF-3 steels are the most resistant, and the molybdenum-containing high-carbon CF-8M steels are the least resistant to embrittlement. Embrittlement of cast stainless steels results in brittle fracture associated with either cleavage of the ferrite or separation of the ferrite/austenite phase boundary. Predominantly brittle failure occurs when either the ferrite phase is continuous, e.g., in cast material with a large ferrite content, or the ferrite/austenite phase boundary provides an easy path for crack propagation, e.g., in high-C grades of cast steel with large phase-boundary carbides. Consequently, the amount, size, and distribution of the ferrite phase in the duplex structure and the presence of phase-boundary carbides are important parameters in controlling the degree or extent of embrittlement.

Thermal aging of cast stainless steels at 300–450°C leads to precipitation of additional phases in the ferrite matrix, e.g., formation of a Cr-rich α' phase by spinodal decomposition; nucleation and growth of α'; precipitation of Ni- and Si-rich G phase, $M_{23}C_6$, and γ_2 (austenite); and additional precipitation and/or growth of existing carbides at the ferrite/austenite phase boundaries. The additional phases provide the strengthening mechanisms that increase strain hardening and local tensile stress. Consequently, the critical stress level for brittle fracture is achieved at higher temperatures. The effects of material variables on the embrittlement of cast stainless steels have been evaluated.

This report presents Charpy-impact data on several experimental and commercial heats of cast stainless steel that were aged up to 30,000 h at 290–450°C. The results indicate that, for a specific cast stainless steel, the extent of embrittlement, i.e., the minimum room-temperature impact energy that would be achieved after long-term aging, depends on the chemical composition and ferrite morphology of the steel. A correlation is presented for estimating the extent of embrittlement from known material information. The extent and rate of embrittlement depend on material parameters, i.e., ferrite morphology and chemical composition of the steel. Ferrite morphology strongly affects the extent of embrittlement, whereas material composition influences the kinetics of embrittlement. Small changes in the constituent elements of the cast material can cause the kinetics of embrittlement to vary significantly.

Annealing studies indicate that the degradation in mechanical properties due to thermal embrittlement can be reversed by annealing the embrittled material for 1 h at 550°C and then water quenching. The kinetics of embrittlement can also be obtained from aging studies on the reembrittlement of recovery-annealed material. This procedure may be useful for establishing baseline mechanical properties and kinetics of embrittlement of service-aged components.

1 Introduction

A program is being conducted to investigate the significance of low-temperature embrittlement of cast duplex stainless steels under light-water reactor (LWR) operating conditions and to evaluate possible remedies for embrittlement problems in existing and future plants. The scope of the program includes the following goals: (1) characterize and correlate the microstructure of in-service reactor components and laboratory-aged material with loss of fracture toughness to establish the mechanism of aging and validate the simulation of in-reactor degradation by accelerated aging, (2) establish the effects of key compositional and metallurgical variables on the kinetics and extent of embrittlement, and (3) develop the methodology and correlations for predicting the toughness loss suffered by cast stainless steel components during normal and extended life of LWRs.

Microstructural and mechanical-property data are being obtained on 25 experimental heats (19 in the form of static-cast keel blocks and 6 in the form of 76-mm slabs) and 6 commercial heats (centrifugally cast pipes and a static-cast pump impeller and pump casing ring) as well as reactor-aged material of grades CF-3, CF-8, and CF-8M cast stainless steel. Specimen blanks for Charpy-impact, tensile, and J-R curve tests are being aged at 290, 320, 350, 400, and 450°C for times up to 50,000 h. The reactor-aged material is from the recirculating-pump cover plate assembly of the KRB reactor, which was in service in Gundremmingen, West Germany, for ≈12 yr (≈8 yr at a service temperature of 284°C). Fractured impact test bars from five heats of aged cast stainless steel were obtained from the Georg Fischer Co. (GF) of Switzerland for microstructural characterization. The materials from GF are from a previous study of long-term aging behavior of cast stainless steel.[1] The data on chemical composition, ferrite content, hardness, ferrite morphology, and grain structure of the experimental and commercial heats have been reported earlier.[2-6] The chemical composition, hardness, and ferrite content and distribution of some of the cast materials are given in Table 1. The results of microstructural characterization and mechanical-property data from Charpy-impact, tensile, and J-R curve tests on 16 heats of cast stainless steel aged up to 30,000 h at temperatures between 290 and 450°C have also been presented earlier.[7-15] A preliminary assessment of the processes and significance of thermal aging in cast stainless steels were also presented.[10-12]

The results indicate that thermal aging at temperatures below 500°C increases the tensile strength and decreases the impact energy and fracture toughness of the steels. The Charpy transition curve shifts to higher temperatures. Different heats exhibit different degrees of embrittlement. For cast stainless steel of all grades, the extent of embrittlement increases with an increase in ferrite content. The low-C CF-3 steels are the most resistant, and the Mo-containing, high-C CF-8M steels are the least resistant to embrittlement.

The mechanisms of embrittlement of cast duplex stainless steel have been discussed.[12] Embrittlement of cast stainless steel results in brittle fracture associated with either cleavage of the ferrite or separation of the ferrite/austenite phase boundary (Fig. 1). The degree of embrittlement is controlled by the amount of brittle fracture. Cast stainless steels with poor impact strength exhibit >80% brittle fracture. In some cast steels, a fraction of the material may fail in a brittle fashion but the surrounding austenite provides ductility and toughness. Such steels have adequate impact strength even after long-term aging.

Table 1. Product form, chemical composition, hardness, and ferrite morphology of various heats of cast stainless steel

Heat	Grade	Chemical Composition (wt.%)									Ferrite[a] (%)		Hardness	Ferrite Spacing
		Mn	Si	P	S	Mo	Cr	Ni	N	C	Calc.	Meas.	R_B	(μm)
							Keel Blocks[b]							
50	CF-3	0.60	1.10	0.016	0.007	0.33	17.89	9.14	0.079	0.034	3.0	4.4	80.1	194
49	CF-3	0.60	0.95	0.010	0.007	0.32	19.41	10.69	0.065	0.010	4.4	7.2	76.6	185
48	CF-3	0.60	1.08	0.009	0.006	0.30	19.55	10.46	0.072	0.011	5.1	8.7	78.1	127
47	CF-3	0.60	1.06	0.007	0.006	0.59	19.81	10.63	0.028	0.018	8.4	16.3	79.7	68
52	CF-3	0.57	0.92	0.012	0.005	0.35	19.49	9.40	0.052	0.009	10.3	13.5	81.6	69
51	CF-3	0.63	0.86	0.014	0.005	0.32	20.13	9.06	0.058	0.010	14.3	18.0	83.8	52
58	CF-8	0.62	1.12	0.010	0.005	0.33	19.53	10.89	0.040	0.056	3.2	2.9	77.1	303
54	CF-8	0.55	1.03	0.011	0.005	0.35	19.31	9.17	0.084	0.063	4.1	1.8	83.3	317
57	CF-8	0.62	1.08	0.009	0.004	0.34	18.68	9.27	0.047	0.056	4.4	4.0	80.2	138
53	CF-8	0.64	1.16	0.012	0.009	0.39	19.53	9.23	0.049	0.065	6.3	8.7	83.1	92
56	CF-8	0.57	1.05	0.007	0.007	0.34	19.65	9.28	0.030	0.066	7.3	10.1	82.5	84
59	CF-8	0.60	1.08	0.008	0.007	0.32	20.33	9.34	0.045	0.062	8.8	3.5	83.2	75
61	CF-8	0.65	1.01	0.007	0.007	0.32	20.65	8.86	0.080	0.054	10.0	13.1	85.3	82
60	CF-8	0.67	0.95	0.008	0.006	0.31	21.05	8.34	0.058	0.064	15.4	21.1	86.7	63
62	CF-8M	0.72	0.56	0.007	0.005	2.57	18.29	12.39	0.030	0.063	2.8	4.5	78.1	140
63	CF-8M	0.61	0.58	0.007	0.006	2.57	19.37	11.85	0.031	0.055	6.4	10.4	81.6	81
66	CF-8M	0.60	0.49	0.012	0.007	2.39	19.45	9.28	0.029	0.047	19.6	19.8	85.3	41
65	CF-8M	0.50	0.48	0.012	0.007	2.57	20.78	9.63	0.064	0.049	20.9	23.4	89.0	43
64	CF-8M	0.60	0.63	0.006	0.005	2.46	20.76	9.40	0.038	0.038	29.0	28.4	89.7	41
							76-mm Slabs[c]							
69	CF-3	0.63	1.13	0.015	0.005	0.34	20.18	8.59	0.028	0.023	21.0	23.6	83.7	35
73	CF-8	0.72	1.09	0.028	0.016	0.25	19.43	8.54	0.053	0.070	7.0	7.7	78.8	253
68	CF-8	0.64	1.07	0.021	0.014	0.31	20.64	8.08	0.062	0.063	14.9	23.4	84.6	87
70	CF-8M	0.55	0.72	0.021	0.016	2.30	19.17	9.01	0.049	0.066	14.2	18.9	86.5	96
74	CF-8M	0.54	0.73	0.022	0.016	2.51	19.11	9.03	0.048	0.064	15.5	18.4	85.8	90
75	CF-8M	0.53	0.67	0.022	0.012	2.58	20.86	9.12	0.052	0.065	24.8	27.8	89.5	69
							Reactor Components[d]							
P3	CF-3	1.06	0.88	0.017	0.014	0.01	18.89	8.45	0.168	0.021	2.8	1.9	82.2	–
P2	CF-3	0.74	0.94	0.019	0.006	0.16	20.20	9.38	0.040	0.019	12.5	15.6	83.8	69
I	CF-3	0.47	0.83	0.030	0.011	0.45	20.20	8.70	0.032	0.019	20.4	17.1	81.0	65
C1	CF-8	1.22	1.18	0.033	0.008	0.65	19.00	9.37	0.040	0.039	7.8	2.2	79.5	–
P1	CF-8	0.59	1.12	0.026	0.013	0.04	20.49	8.10	0.056	0.036	17.7	24.1	84.9	90
P4	CF-8M	1.07	1.02	0.019	0.015	2.05	19.64	10.00	0.151	0.040	5.9	10.0	83.1	182
205	CF-8M	0.93	0.63	0.019	–	3.37	17.88	8.80	–	0.040	21.0	15.9	–	79
758	CF-8M	0.91	0.62	0.018	–	3.36	17.91	8.70	–	0.030	24.2	19.2	–	62
							Reactor-Aged[e]							
KRB	CF-8	0.31	1.17	–	–	0.17	21.99	8.03	0.038	0.062	27.7	34.0	–	–

Table 1. (Contd.)

Heat	Grade	Chemical Composition (wt.%) Mn	Si	P	S	Mo	Cr	Ni	N	C	Ferrite[a] (%) Calc.	Meas.	Hardness R_B	Ferrite Spacing (μm)
							Laboratory-Aged[f]							
280	CF-3	0.50	1.37	0.015	0.006	0.25	21.60	8.00	0.038	0.028	36.3	40.0	–	186
278	CF-8	0.28	1.00	0.008	0.019	0.13	20.20	8.27	0.030	0.038	18.5	15.0	–	174
292	CF-8	0.34	1.57	0.018	0.016	0.13	21.60	7.52	0.039	0.090	23.9	28.0	–	–
286	CF-8M	0.40	1.33	0.044	0.015	2.44	20.20	9.13	0.062	0.072	18.9	22.0	–	201

[a] Calculated from the composition with Hull's equivalent factor.
Measured by ferrite scope AUTO Test FE, Probe Type FSP-1.
[b] *Static Cast Keel Blocks:* Foundry ESCO; Size 180 x 120 x 90-30 mm.
[c] *Static Cast Slabs*: Foundry ESCO; Size 610 x 610 x 76 mm.
[d] *Centrifugally Cast Pipes*:
P3 Foundry SANDUSKY; Size 580 mm O.D.,76 mm wall.
P2 Foundry FAM, France; Size 930 mm O.D., 73 mm wall.
P1 Foundry ESCO; Size 890 mm O.D., 63 mm wall.
P4 Foundry SANDUSKY; Size 580 mm O.D., 32 mm wall.
205 Size 305 mm O.D., 25 mm wall.
Static Cast:
Elbow 758: Size 305 mm O.D., 30 mm wall.
Pump Impeller I: Foundry ESCO; Size 660 mm diameter.
Pump Casing C1: Foundry ESCO; Size 600 mm O.D., 57 mm wall.
[e] *KRB Reactor Pump Cover Plate*: Foundry GF; Size 890 mm diameter.
[f] *Aged Material from George Fischer Co., Switzerland.*

Predominantly brittle failure occurs when either the ferrite phase is continuous, e.g., in cast material with a large ferrite content, or the ferrite/austenite phase boundary provides an easy path for crack propagation, e.g., in high-C cast steels with large phase-boundary carbides. Consequently, the amount, size, and distribution of the ferrite phase in the duplex structure, and the presence of phase-boundary carbides are important parameters in controlling the degree or extent of embrittlement.

Thermal aging of cast stainless steels at 300-450°C leads to precipitation of additional phases in the ferrite matrix, e.g., formation of a Cr-rich α' phase by spinodal decomposition; nucleation and growth of α'; precipitation of an Ni- and Si-rich G phase, $M_{23}C_6$, and γ_2 (austenite); and additional precipitation and/or growth of existing carbides at the ferrite/austenite phase boundaries.[13-15] The additional phases provide the strengthening mechanisms that increase strain hardening and local tensile stress. Consequently, the critical stress level for brittle fracture is achieved at higher temperatures.

Phase-boundary separation generally occurs in the high-C steels because of the presence of large $M_{23}C_6$ at the phase boundaries. For CF-8 steels, the phase-boundary carbides form during production heat treatment of the casting. Consequently, the unaged CF-8 steels exhibit low lower-shelf energy and high mid-shelf Charpy transition temperature (CTT) relative to the CF-3 steels. The fracture mode of CF-8 steels in the lower-shelf or transition-temperature regime is predominantly phase-boundary separation;[7,8] in contrast, the CF-3 steels show dimpled ductile failure. Fracture by phase-boundary separation is observed in only a few heats of unaged CF-8M steels and is dependent on whether the material contains phase-boundary carbides. The difference in fracture mode is reflected in yield and maximum loads obtained from the load-time traces of the instrumented Charpy tests.

The results for unaged and aged Heats 68 (CF-8) and 69 (CF-3) are shown in Fig. 2. The estimated yield and ultimate tensile stresses[7,8] can be determined from the axes on the right side of the figures. The results indicate the expected decrease in yield and maximum loads with increase in temperature. Thermal aging increases the loads at all temperatures. For Heat 68, the critical stress for brittle fracture is achieved before general yielding at temperatures up to room temperature; the maximum and yield loads are the same. Heat 69 shows strain hardening at all temperatures and fractures at higher loads, although the ferrite contents of the two heats are comparable. Failure occurs at ≈16 kN load in Heat 68 and ≈20 kN load in Heat 69. The difference in the maximum loads at failure suggests a difference in fracture mechanism.

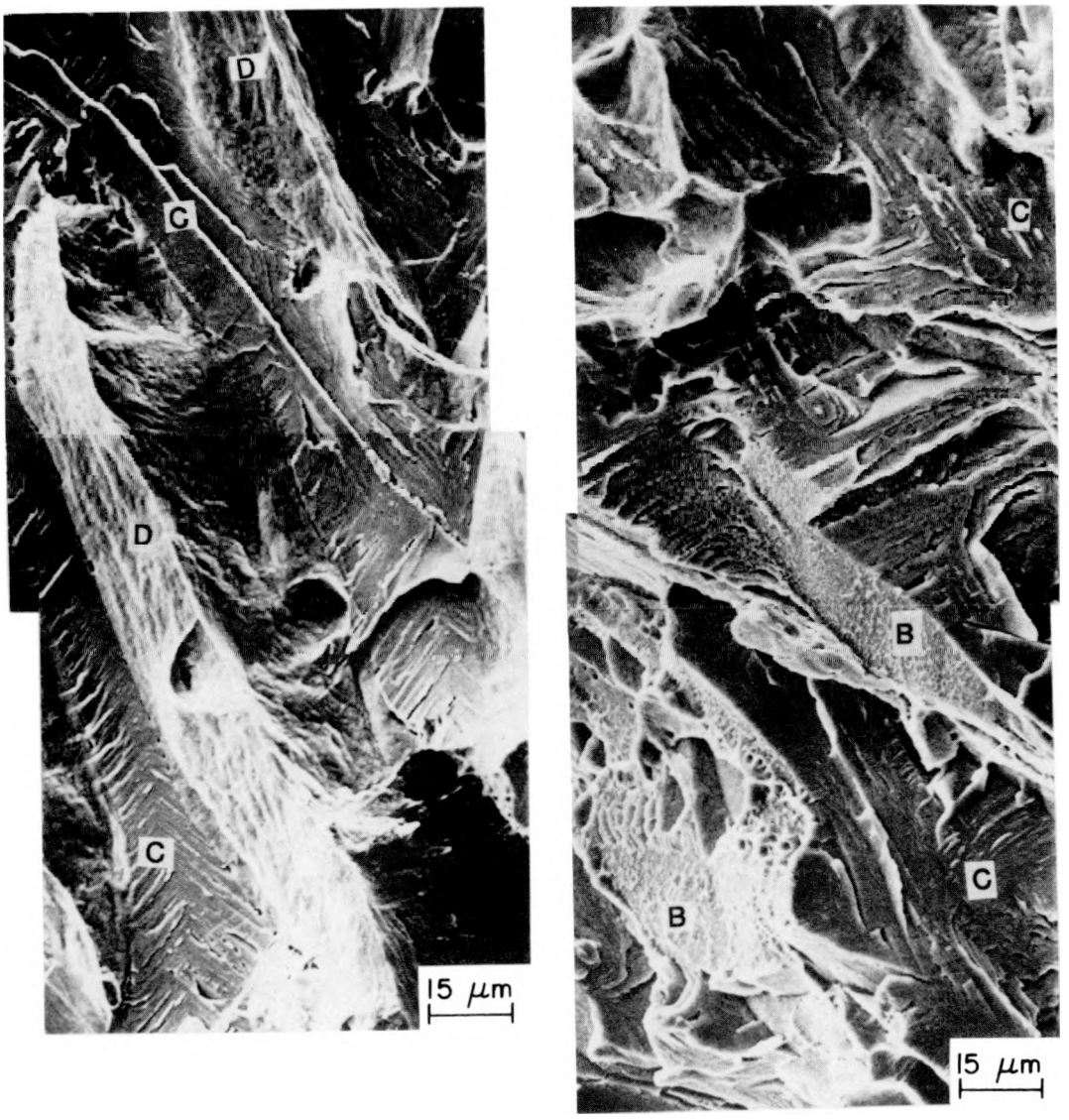

Figure 1. Fracture surfaces of Heat 68 aged for 10,000 h at 400°C and tested at room temperature. Fracture mode B = phase-boundary separation, C = cleavage of ferrite, D = ductile failure.

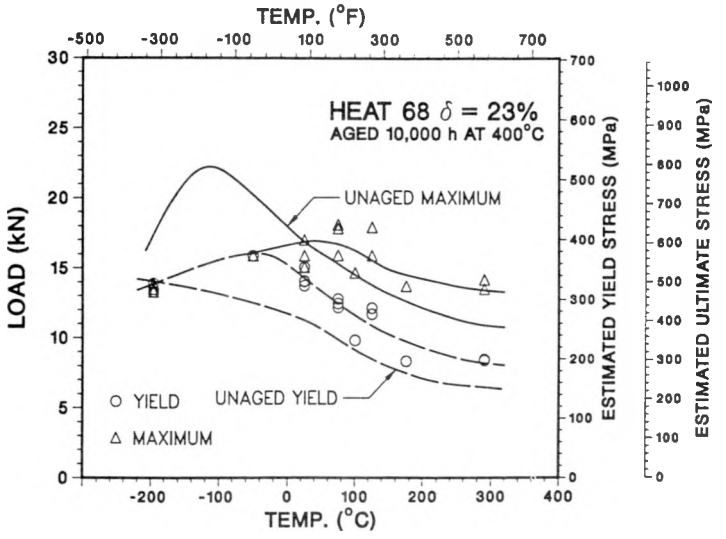

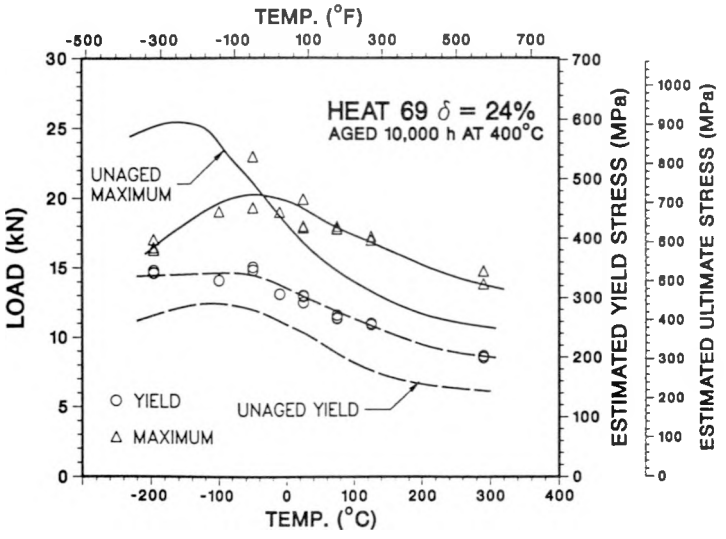

Figure 2. Yield and maximum loads from Charpy-impact tests for Heats 68 and 69, aged for 10,000 h at 400°C

The effects of material variables on the embrittlement of cast stainless steels have been evaluated. The kinetics and extent of embrittlement are controlled by several mechanisms that depend on material parameters and aging temperature. Materials aged at 450°C show significant precipitation of phase-boundary carbides (also nitrides in high-N steels) and a large decrease in ferrite content.[10,12] At reactor temperatures, such processes either do not occur or their kinetics are extremely slow. Consequently, data obtained at 450°C aging do not reflect reactor operating conditions, and extrapolation of these data to predict the extent of embrittlement at reactor temperatures is not valid. The chemical composition of the steel and the ferrite content and spacing are important parameters in controlling the extent and kinetics of embrittlement. Ferrite morphology strongly affects the extent of embrittlement, whereas material composition influences the kinetics of embrittlement. Small changes in the constituent elements of the cast material can cause the kinetics of embrittlement to vary significantly. The kinetics of embrittlement are controlled by spinodal decomposition and precipitation of G phase in ferrite, as well as by precipitation and

growth of phase-boundary carbides. The rate of embrittlement for a specific cast stainless steel depends on the relative contributions of carbide and G-phase precipitation; activation energies can range from 65 to 230 kJ/mole. An initial assessment of the mechanisms and the significance of low-temperature embrittlement of cast stainless steels in LWR systems have been presented.[12]

This report presents Charpy-impact data on several heats of cast stainless steel aged up to 30,000 h at 320, 350, and 400°C. The results are analyzed to establish the kinetics of embrittlement and estimate the extent of embrittlement of cast stainless steels from known material parameters.

2 Mechanical Properties

2.1 Room-Temperature Impact Energy

The Charpy-impact data for various experimental and commercial heats, aged up to 30,000 h at 290, 320, 350, 400, and 450°C, were presented in Ref. 12. The results from room-temperature Charpy-impact tests were analyzed to determine the kinetics and extent of embrittlement. The variation of Charpy-impact energy C_V (J/cm^2) with time can be expressed as

$$\log_{10}C_V = \log_{10}C_{Vsat} + \beta\{1 - \tanh [(P - \theta)/\alpha]\}, \quad (1)$$

where P is the aging parameter, C_{Vsat} (J/cm^2) is the minimum impact energy reached after long-term aging, β is half the maximum decrease in impact energy, θ is the log of the time to achieve β reduction in impact energy, and α is a shape factor. The aging parameter represents the time to achieve a specific degree of aging at 400°C. The aging time to reach a given degree of embrittlement at different temperatures is determined from the equation

$$t = 10^P \exp\left[\frac{Q}{R}\left(\frac{1}{T} - \frac{1}{673}\right)\right], \quad (2)$$

where Q is the activation energy, R is the gas constant, T is the absolute temperature, and P is the aging parameter that represents the degree of aging reached after 10^P h at 400°C.

The mechanical-property data indicate that the kinetics and extent of embrittlement are controlled by several mechanisms that depend on material parameters and aging temperature. Precipitation of phase-boundary carbides and/or growth of existing carbides occurs in CF-8 and CF-8M steels during aging at 400 and 450°C. The fracture surfaces of Charpy-impact specimens of Heat 60, unaged and aged at 400 and 450°C and tested at −197°C, are shown in Fig. 3. The fracture mode of the specimen aged at 450°C is predominantly phase-boundary separation. Furthermore, thermal aging at 450°C leads to substantial decrease in ferrite content of the steel (Fig. 4). At reactor temperatures, such processes either do not occur or their kinetics are extremely slow. Because the data obtained after 450°C aging are not representative of reactor operating conditions, they were excluded from the analysis. The Charpy data obtained after 290°C aging showed no reduction in impact energy even after aging for 30,000 h; instead, a slight increase in impact energy was observed relative to the unaged material. This increase in impact energy is real and was

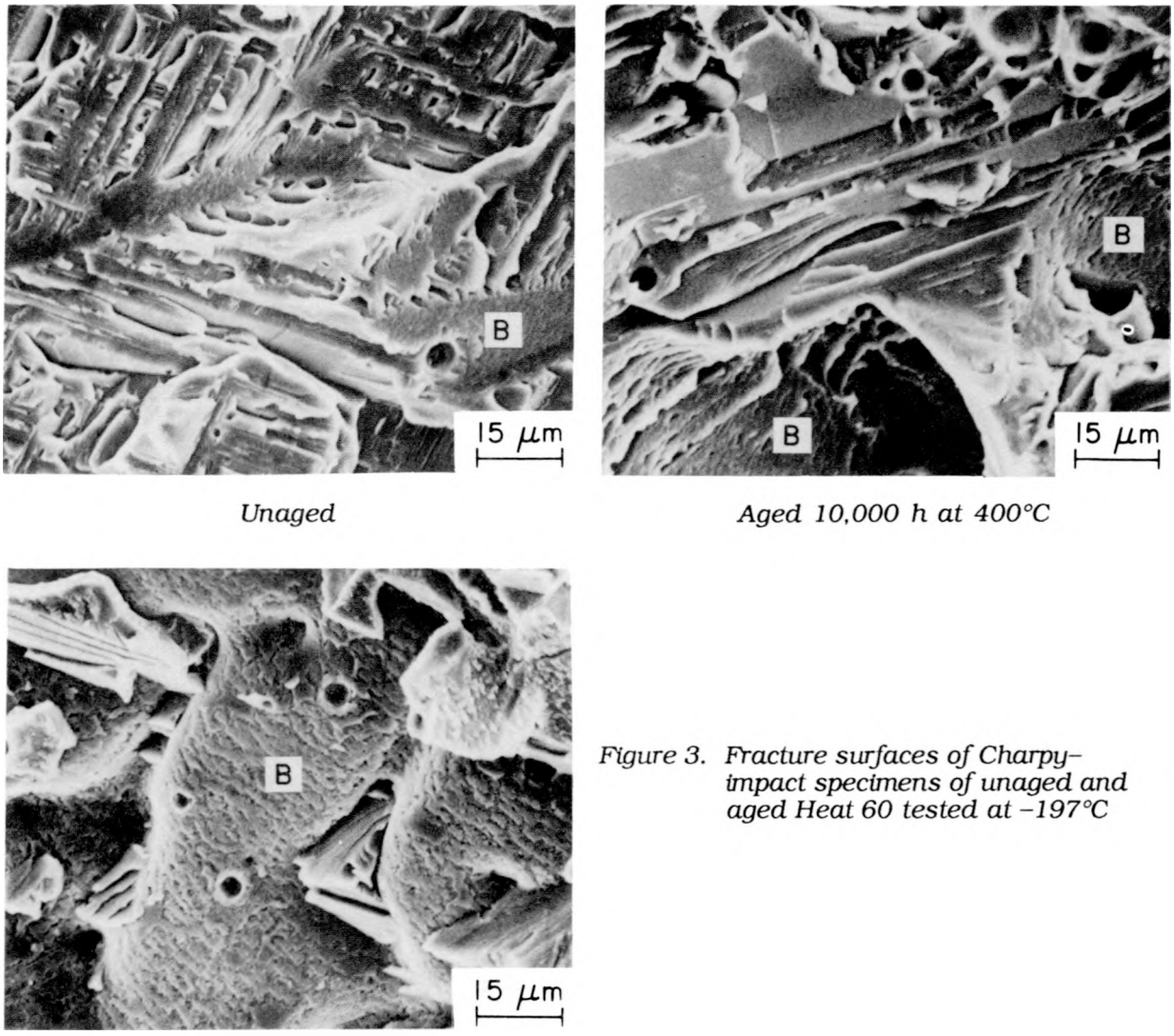

Unaged

Aged 10,000 h at 400°C

Aged 10,000 h at 450°C

Figure 3. Fracture surfaces of Charpy-impact specimens of unaged and aged Heat 60 tested at −197°C

observed for most heats aged at low temperatures, i.e., aged up to 30,000 h at 290°C or up to 10,000 h at 320°C. The data from the relatively short-time aging at 290°C tend to bias the analyses to yield higher values of activation energies; therefore, the 290°C aging results were also excluded from the analysis.

The values of the constants in Eqs. 1 and 2 were obtained from best fit of the Charpy data for various heats of cast stainless steel aged up to 30,000 h at 320, 350, and 400°C. Activation energies, with the 95% confidence limits, are given in Table 2. The confidence limits are large for some heats because of the relatively small decrease in impact energy and large scatter in the data. The Charpy-impact data for three heats are plotted as a function of aging time in Fig. 5, along with the fitted curves determined from Eqs. 1 and 2.

The activation energies reported earlier[10,12] primarily represent the kinetics of embrittlement at temperatures between 400 and 350°C. Charpy data for long-term aging (i.e., 30,000 h) at 320°C were not included in the analyses. The earlier values are 15–20% lower than those determined from aging data at temperatures between 400 and 320°C. The

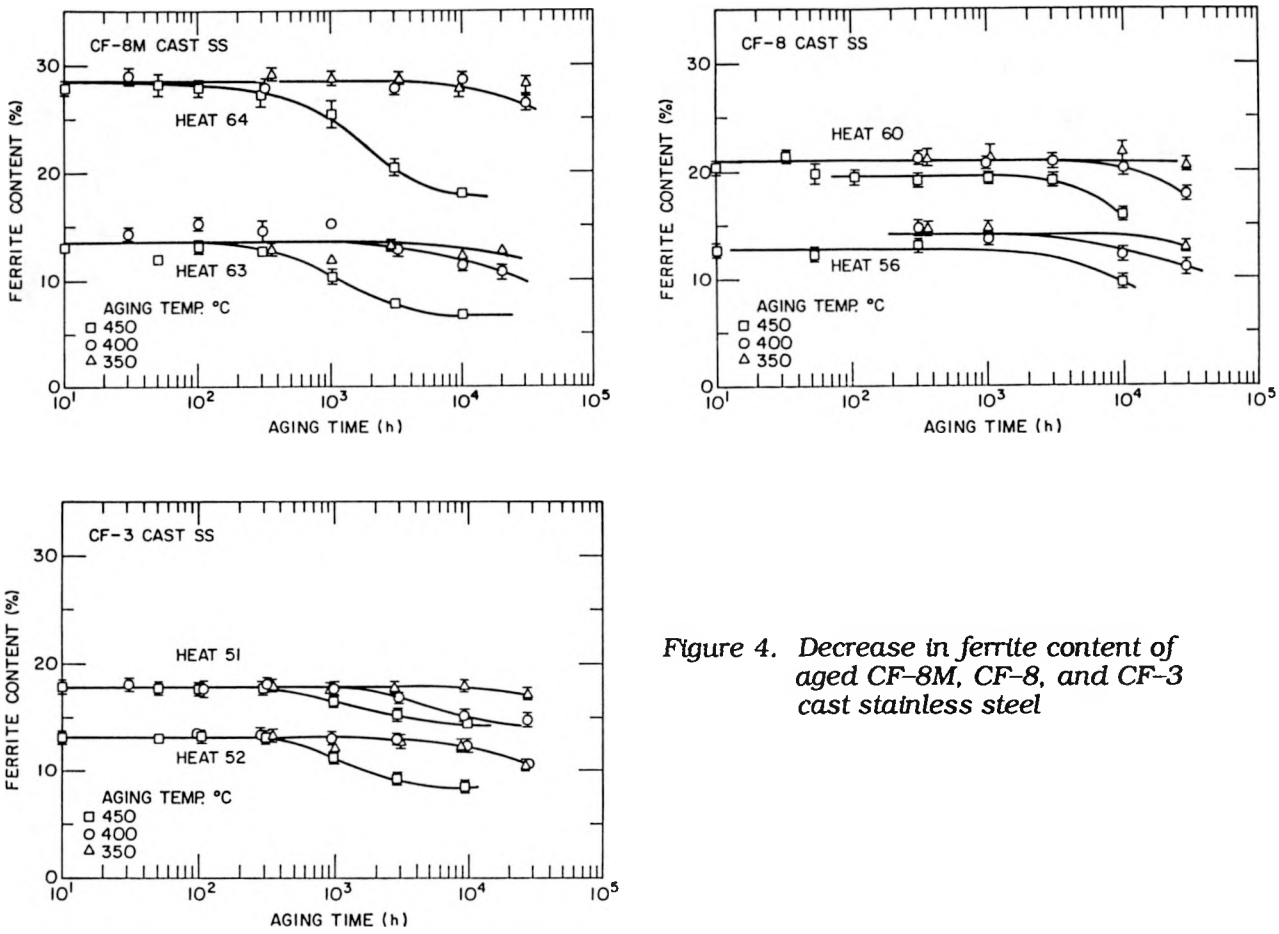

Figure 4. Decrease in ferrite content of aged CF-8M, CF-8, and CF-3 cast stainless steel

Table 2. Activation energies for kinetics of embrittlement of cast stainless steels

Heat	Parameter Φ[a]	Cv_{sat} (J/cm^2)	Constants β	θ	α	Q {kJ/mole (kcal/mole)} Average	95% Confidence Limit
47	12.0	174.2	0.063	2.35	1.40	187 (44.7)	73–300 (17.5–71.8) [b]
51	10.8	149.2	0.083	3.00	0.76	221 (52.8)	123–320 (29.3–76.4) [b]
69	12.4	96.9	0.202	3.05	0.93	167 (40.0)	120–215 (28.7–51.3) [b]
59	22.2	99.8	0.166	3.12	1.40	229 (54.7)	156–301 (37.4–72.0)
60	45.5	52.0	0.288	2.95	0.89	227 (54.2)	186–267 (44.4–63.9)
68	74.4	46.4	0.348	3.00	0.74	169 (40.5)	136–204 (32.4–48.2)
P1	53.5	58.7	0.282	2.38	0.75	249 (59.6)	210–289 (50.2–69.1)
63	15.8	111.7	0.155	3.20	1.40	119 (28.4)	67–170 (16.0–40.7)
64	39.4	45.2	0.304	2.75	0.62	156 (37.4)	131–181 (31.4–43.2)
65	40.3	58.5	0.269	2.93	0.94	191 (45.7)	154–228 (36.8–54.6)
66	19.5	106.3	0.149	3.02	1.30	203 (48.4)	125–280 (29.9–66.9) [b]
75	106.4	34.7	0.422	2.76	0.53	146 (34.8)	127–165 (30.3–39.4)
P4	41.5	53.8	0.325	2.95	0.89	143 (34.2)	115–171 (27.6–40.8)

[a] Calculated from Eq. 4.
[b] Standard deviation is large because of the relatively small decrease in impact energy and a large scatter in data.

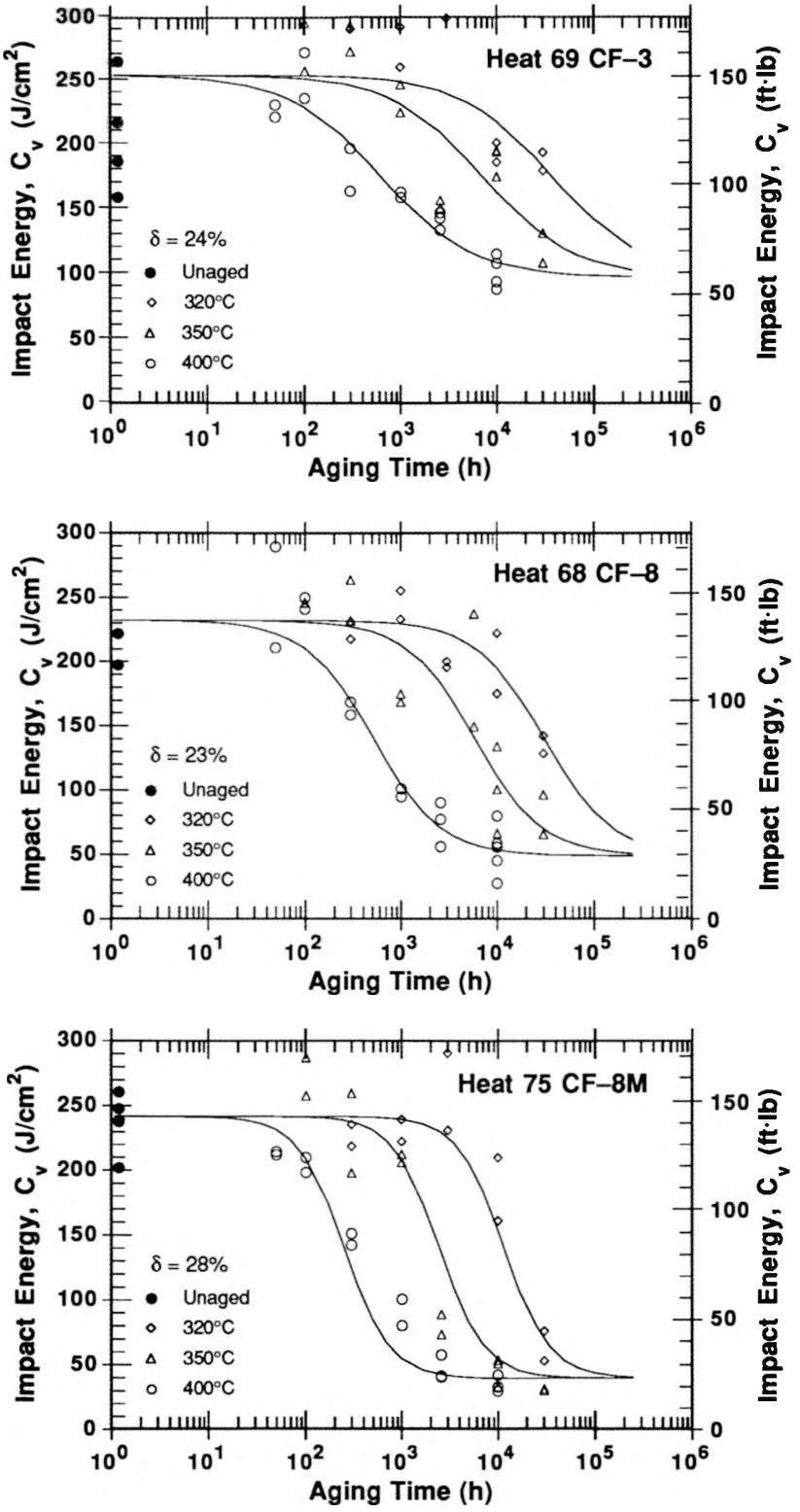

Figure 5. Effect of thermal aging on room-temperature impact energy of CF-3, CF-8, and CF-8M cast stainless steel

results suggest that the activation energy for embrittlement is not constant in the temperature range of 290–400°C, but increases with decrease in temperature. Similar behavior has been reported for several heats of CF–8M steels aged at temperatures between 300 and 400°C.[16] Consequently, extrapolation of the 400°C data to reactor temperatures by applying activation energies obtained from 350–400°C aging would yield conservative estimates of embrittlement for some of the heats of cast stainless steel.

2.2 Extent of Embrittlement

Charpy–impact data obtained at room temperature were analyzed to develop a correlation between material variables and the extent or degree of embrittlement, i.e., the minimum room–temperature impact energy, C_{Vsat} in Eq. 1, that could be achieved after long–term aging. It is well established that the extent of embrittlement increases with an increase in the ferrite content of cast stainless steel. Furthermore, Charpy–impact data for several heats of CF–8 and CF–8M steels aged for 10,000 h at 350 or 400°C indicate that the impact energy decreases with an increase in the Cr content, irrespective of the ferrite content in the steel.[16] A better correlation was obtained when the total concentration of ferrite formers (i.e., Cr, Mo, and Si) was considered.[16] A sharp decrease in impact energy occurs when either the Cr content exceeds 18 wt.% or the concentration of Cr+Mo+Si exceeds 23.5 wt.%. An increase in the concentration of C or N in the steel also increases the extent of embrittlement because of the contribution to phase–boundary carbides or nitrides and the subsequent fracture by phase–boundary separation. The influence of C content on the extent of embrittlement is clearly seen in Fig. 5. Although the ferrite content and concentrations of Cr+Mo+Si are comparable for Heats 68 and 69, the minimum impact energy for Heat 68 (CF–8) is significantly lower than that for Heat 69 (CF–3).

The data on the minimum room–temperature impact energy C_{Vsat} (J/cm^2) were analyzed with an exponential function of the various material variables. The best fit of the data was obtained with the expression

$$\log_{10}C_{Vsat} = 1.386 + 0.938\exp(-0.0205\Phi). \quad (3)$$

The material parameter Φ is given by

$$\Phi = \delta_m^2(Cr + Mo + Si)(C + 0.4N)Ni\lambda/10^4, \quad (4)$$

where δ_m, the measured ferrite content, is in %, the concentrations of Cr, Mo, Si, C, and N are in wt.%, and the mean ferrite spacing λ is in μm. A similar correlation, but without the effect of ferrite spacing, was proposed earlier by investigators at Electricité de France (EdF).*

Minimum impact energy is plotted as a function of the material parameter Φ in Fig. 6. Results from the studies at Framatome (FRA),[17,18] Central Electricity Generating Board (CEGB),[19] and Electric Power Research Institute (EPRI)[20] are also shown in the figure. The data show good correlation with the material parameter. However, the impact energy for

*M. Guttmann, EdF, private communication, October 1987.

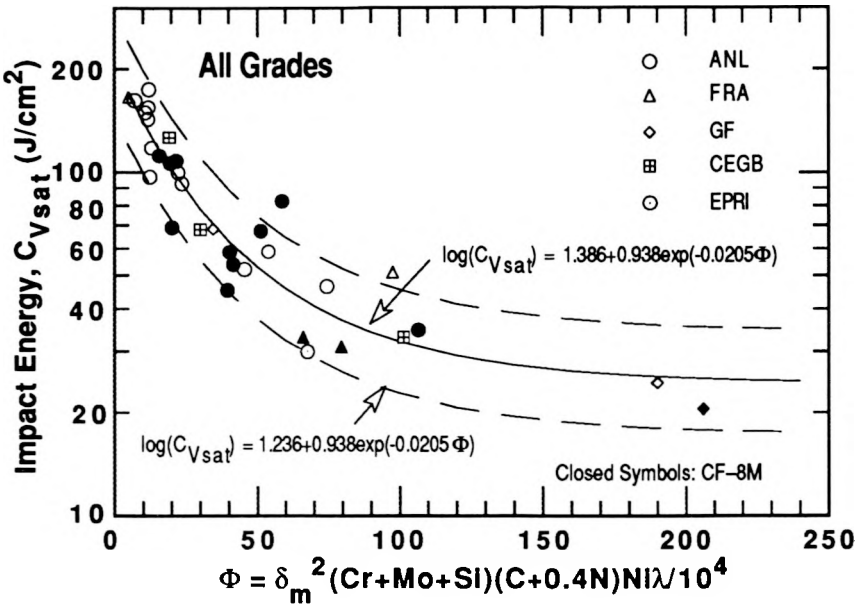

Figure 6. Correlation between minimum room-temperature impact energy and material parameter Φ for aged cast stainless steel. The curves shown by dashed lines represent ±41% deviation from predicted values.

FRA Heat 4331 (not shown), which contains 0.2 wt.% Nb, was significantly lower than that predicted by Eq. 3. The fracture surface of the impact test specimen of FRA Heat 4331 (Fig. 7) shows large Nb carbides at the phase boundaries. The presence of phase-boundary carbides alters the deformation and fracture behavior of the material, i.e., cleavage can be initiated by carbide cracking. A difference in the mode of fracture is reflected in the values of the yield and maximum loads for the instrumented Charpy tests, shown in Fig. 8 for FRA Heat 4331 and ANL Heat 74. The corresponding Charpy transition curves are shown in Fig. 9. Both heats are CF-8M grade and contain ≈20% ferrite, yet the transition curves are significantly different. The 65-J transition temperature is 220°C for Heat 4331, aged for 700 h at 400°C, and is 20°C for Heat 74 aged for 10,000 h at 400°C. The yield loads are

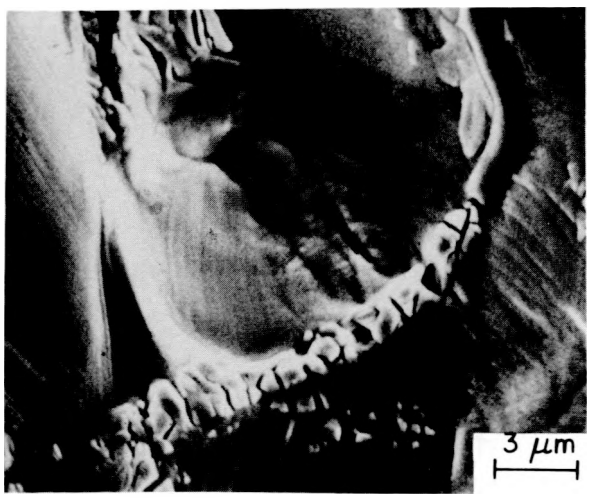

Figure 7. Fracture surface of Charpy-impact specimen of Framatome Heat 4331, aged for 700 h at 400°C

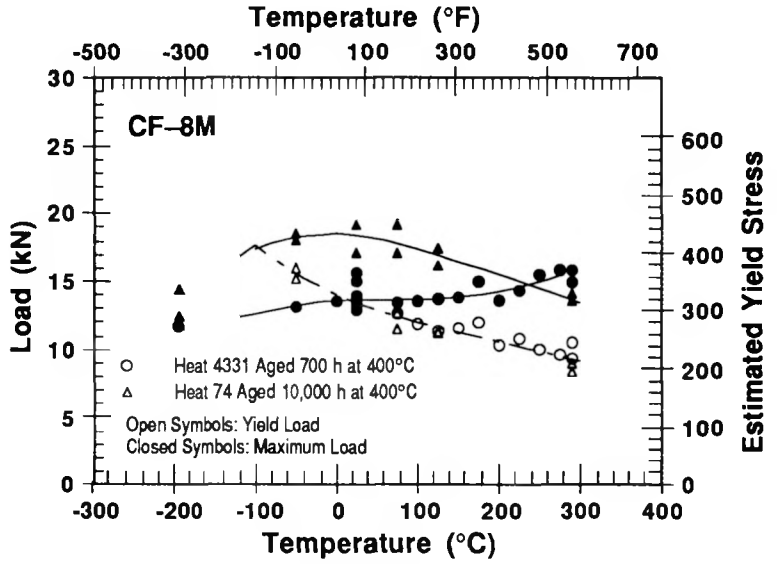

Figure 8. Yield and maximum loads from Charpy-impact data for Framatome Heat 4331 and ANL Heat 74

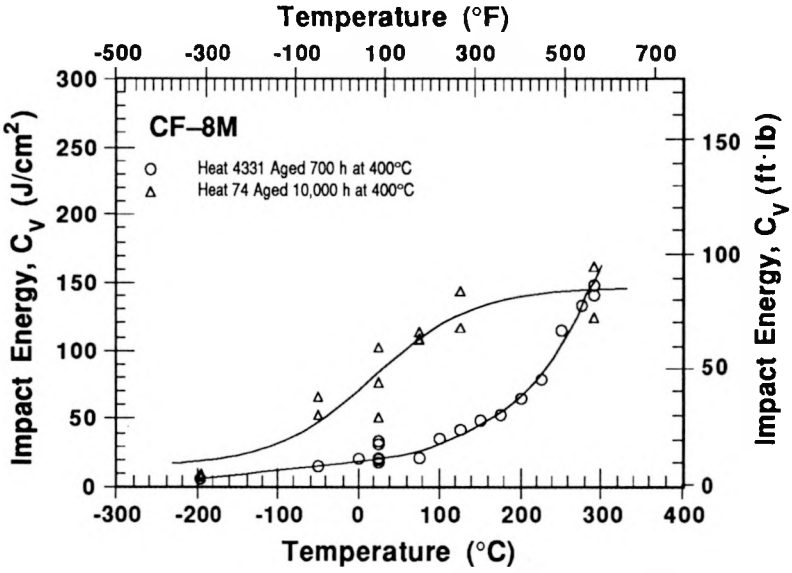

Figure 9. Charpy transition curves for Heats 4331 and 74 aged at 400°C

comparable for both heats, which indicates a similar degree of strengthening in the two heats. However, Fig. 8 shows that failure occurs at ≈14 kN load in Heat 4331 and at ≈18 kN load in Heat 74. The difference in the maximum load at failure suggests a difference in the fracture mechanism. The present correlation does not consider the effects of Nb on embrittlement.

The correlation in Fig. 6 indicates that the impact energy will be less than 50 J/cm^2 for cast stainless steels in which the material parameter is greater than ≈50. For cast stainless steels containing >10% ferrite, mean ferrite spacing is in the range of 40–200 μm,

Cr+Mo+Si concentration is ≈22 wt.% for CF–8 or CF–3 and ≈24 wt.% for CF–8M, and N content is typically 0.04 wt.%. Thus, for cast materials with 0.06 wt.% C, 9 wt.% Ni, and 100 μm ferrite spacing, impact energy will be below 50 J/cm^2 when the ferrite content is above 18%. However, cast materials with 10 or 15% ferrite can also reach very low impact strengths with an increase in any one of the variables included in the material parameter Φ. For example, Ni content is often >10 wt.% for CF–8M steels and values of λ as high as 200 μm have been observed for several heats of cast stainless steel (Table 1).

Equations 3 and 4 can be used to estimate the extent of embrittlement at saturation (expressed in terms of room–temperature impact energy) for a specific cast stainless steel component. The variables in the material parameter can be determined nondestructively. The compositions are generally known, and ferrite content can be calculated from the composition or measured with a magne–gage or ferrite scope. Ferrite spacing is the variable that is least readily available, but it can be determined by surface replica techniques. However, a conservative estimate of the possible extent of embrittlement can be obtained by assuming the highest value observed in the material data base, i.e., a spacing of ≈200 μm.

The effect of material parameter Φ on the extent of embrittlement is clearly seen in Fig. 10. The impact energies for several heats with comparable values of Φ are plotted as a function of the aging parameter P. The different temperatures and times of aging are normalized in terms of P by Eq. 2. The results show that the extent of embrittlement increases with an increase in Φ. For each range of Φ there is a saturation value of minimum impact energy. This behavior is independent of the kinetics of embrittlement, e.g., the extent of embrittlement is comparable for Heats 60, P1, 64, 65, and P4, whereas the activation energies range from 140 to 240 kJ/mole. Ferrite content also varies significantly for these heats: 10% for Heat P4 and 28% for Heat 64.

2.3 Charpy Transition Curves

Assessment of the changes in impact strength at reactor operating temperatures requires evaluation of aging effects on Charpy transition curves. The Charpy data were fitted with a hyperbolic tangent function of the form

$$C_V = K_o + B\{1 + \tanh [(T - C)/D]\}, \quad (5)$$

where K_o is the lower–shelf energy, T is the test temperature, B is half the distance between upper–shelf energy (USE) and lower–shelf energy, C is the mid–shelf Charpy transition temperature (CTT) in °C, and D is the half–width of the transition region. The values of the constants in Eq. 5 are given in Table 3. The effect of aging time on the transition curves for the three grades of cast stainless steel is shown in Fig. 11. The effect of aging temperature for cast materials that were aged for 30,000 h is shown in Fig. 12. Thermal aging decreases the impact energy and shifts the transition curves to higher temperatures. The results indicate a "saturation effect" for USE after aging. The values of USE decrease significantly during aging for ≈2600 h at 350°C but do not decrease further with longer aging times. After saturation of USE, the decrease in room–temperature impact energy is due to an increase in CTT, i.e., the value of B in Eq. 5 remains constant and only C and D increase with longer aging times. This behavior is observed at all aging temperatures and for all heats of material. The three heats that were studied contain similar amounts of ferrite,

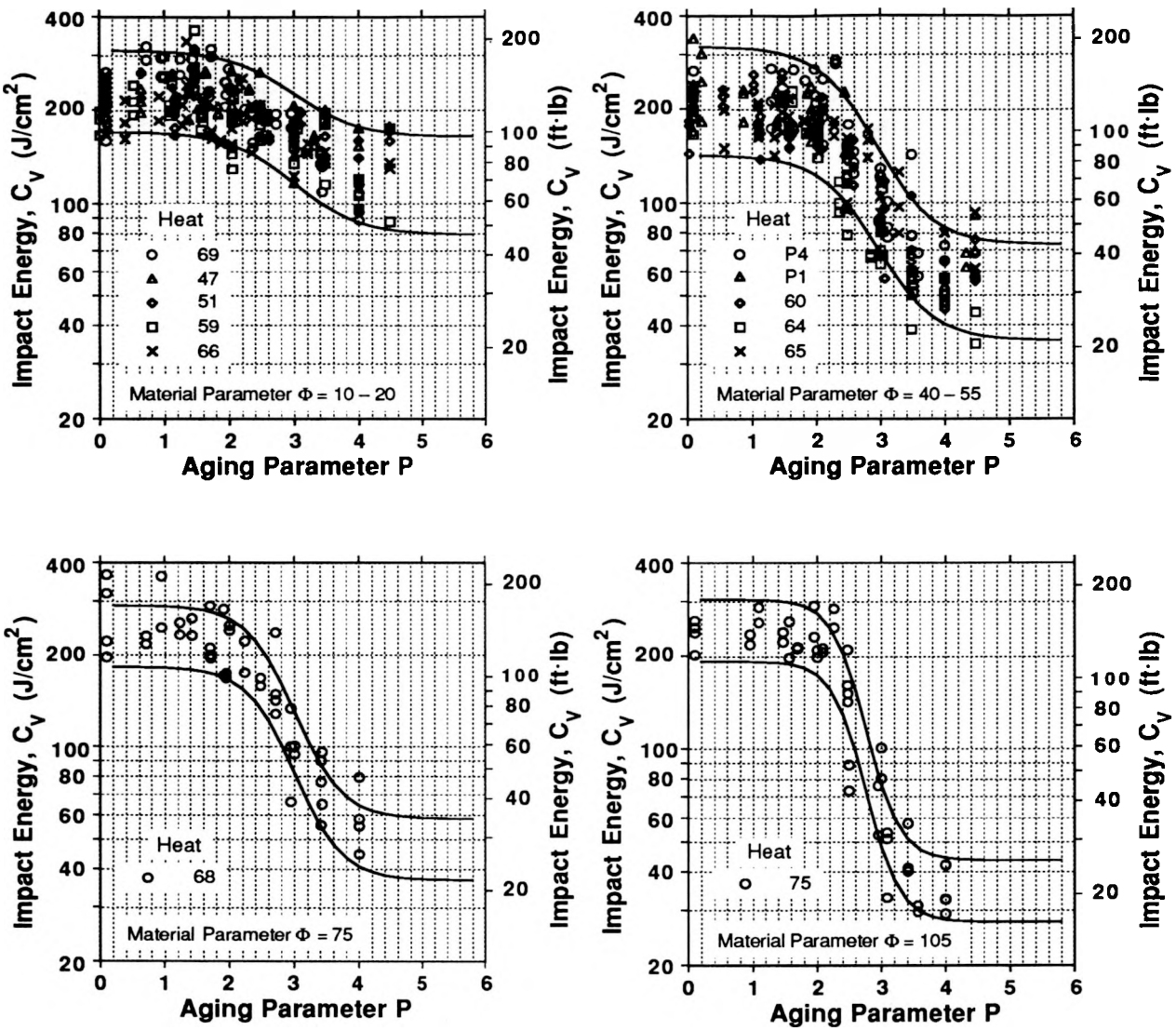

Figure 10. Effect of thermal aging on room-temperature impact energy of CF-3, CF-8, and CF-8M steels with various material parameters Φ

and the saturation values of USE are comparable. However, the shift in CTT is significantly different: the CF-8M steel exhibits the largest shift.

The room-temperature Charpy data (Fig. 5) indicate that for Heats 68, 69, and 75 of cast stainless steel, a saturation value of minimum impact energy is reached after ≈3,000 h at 400°C or ≈30,000 h at 350°C, i.e., when the aging parameter P is ≈3.5. Because both room-temperature impact energy and USE appear to reach saturation values, Charpy transition curves may also show a "saturation effect." Transition curves for three grades of cast stainless steel aged to P values of 3.4–4.0 are shown in Fig. 13. For Heat 69 (Φ ≈ 12), the transition curves for the three aging conditions are comparable. The minimum room-temperature impact energy is close to USE. This suggests a saturation effect on the transition curve, because an increase in CTT would mean a further decrease in room-temperature impact energy. Thus, the curves represent the highest CTT that would be achieved after

Table 3. Values of constants in Eq. 5 for Charpy transition curve of cast stainless steels

Heat	Aging Condition		Constants			
	Temp. (°C)	Time (h)	K_o (J/cm²)	B (J/cm²)	C (°C)	D (°C)
69	Unaged	–	40	130.3	-186.8	222.7
	290	30,000		86.4	-176.8	30.0
	320	10,000		78.2	-154.1	37.8
	320	30,000		90.5	-74.2	89.2
	350	2,570		69.1	-113.2	50.4
	350	10,000		73.5	-34.6	43.5
	350	30,000		59.2	-16.9	107.1
	400	2,570		55.6	-60.7	87.4
	400	10,000		54.7	-16.9	98.0
	450	2,570		50.6	-85.0	126.5
I	Unaged	–	50	62.8	-307.9	106.2
	320	30,000		81.8	-184.0	127.9
	350	9,980		49.8	-125.4	51.7
	400	9,980		44.3	-120.9	70.4
P2	Unaged		50	162.1	-189.0	44.1
	320	30,000		172.7	-42.2	71.9
	350	10,000		148.7	-43.1	87.8
	350	30,000		157.0	-5.8	97.6
68	Unaged	–	15	138.3	-59.8	99.9
	290	30,000		169.0	-12.1	98.4
	320	10,000		97.4	-40.9	46.0
	320	30,000		110.1	-0.9	121.2
	350	5,780		78.5	-12.6	60.7
	350	10,000		97.0	28.0	67.3
	350	30,000		86.3	53.3	85.7
	400	2,570		70.5	31.3	78.5
	400	10,000		68.6	64.0	64.3
	450	2,570		54.9	32.6	86.7
70	Unaged	–	15	119.7	-156.2	60.6
	350	2,570		105.6	-77.0	38.7
	350	10,000		89.2	23.6	121.7
	400	2,570		87.4	-1.7	116.2
	400	10,000		71.2	10.3	90.9
74	Unaged	–	15	89.5	-177.5	119.6
	290	30,000		140.9	-104.8	40.7
	320	10,000		91.1	-95.0	65.8
	320	30,000		87.1	-8.5	84.3
	350	2,570		89.0	-88.7	38.9
	350	10,000		71.5	-35.6	86.7
	350	30,000		81.2	79.4	168.5
	400	2,570		61.6	-37.2	49.6
	400	10,000		65.6	19.2	123.7
	450	2,570		39.2	-47.0	63.5
75	Unaged	–	15	92.0	-156.5	43.7
	290	30,000		121.6	-76.4	50.5
	320	10,000		90.4	-16.0	37.9
	320	30,000		78.4	83.0	140.1
	350	2,570		70.9	-10.2	105.2
	350	10,000		71.3	80.5	74.4
	350	30,000		67.9	207.7	180.1
	400	2,570		52.7	45.5	83.1
	00	10,000		66.3	140.7	138.8
	50	2,570		34.0	20.8	99.4

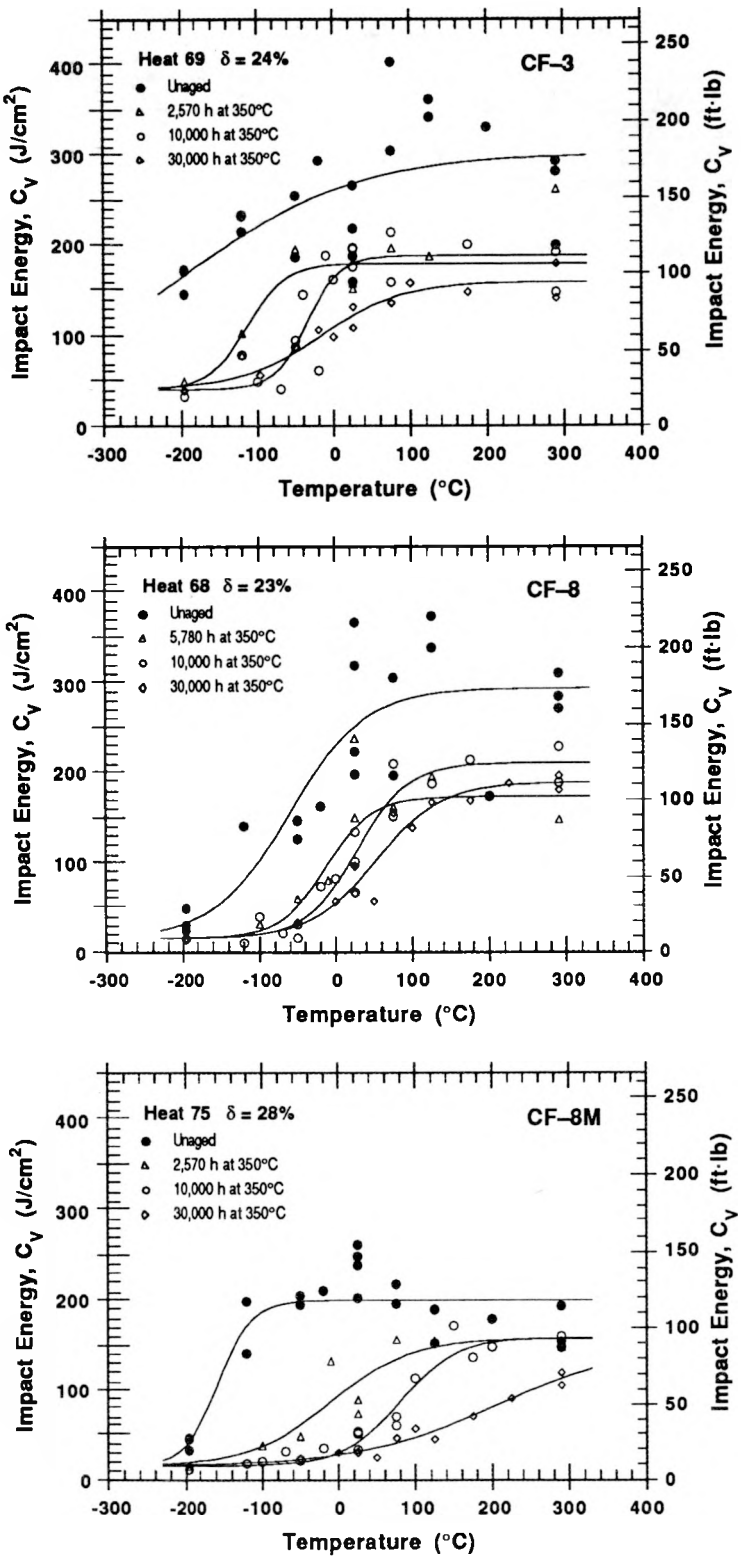

Figure 11. Effect of aging time on Charpy transition curves of CF–3, CF–8, and CF–8M steels aged at 350°C

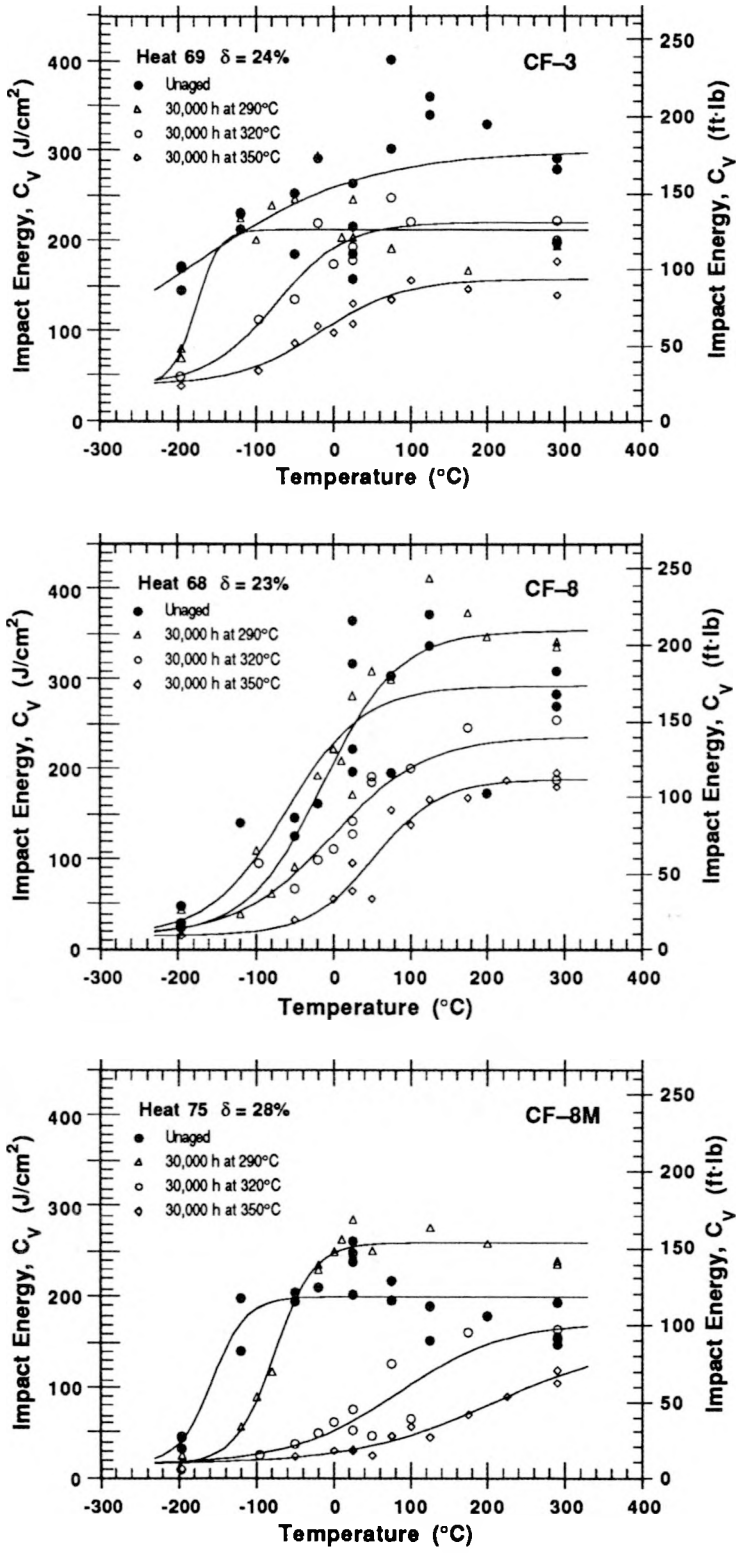

Figure 12. Effect of temperature on Charpy transition curves of CF-3, CF-8, and CF-8M steels aged for 30,000 h

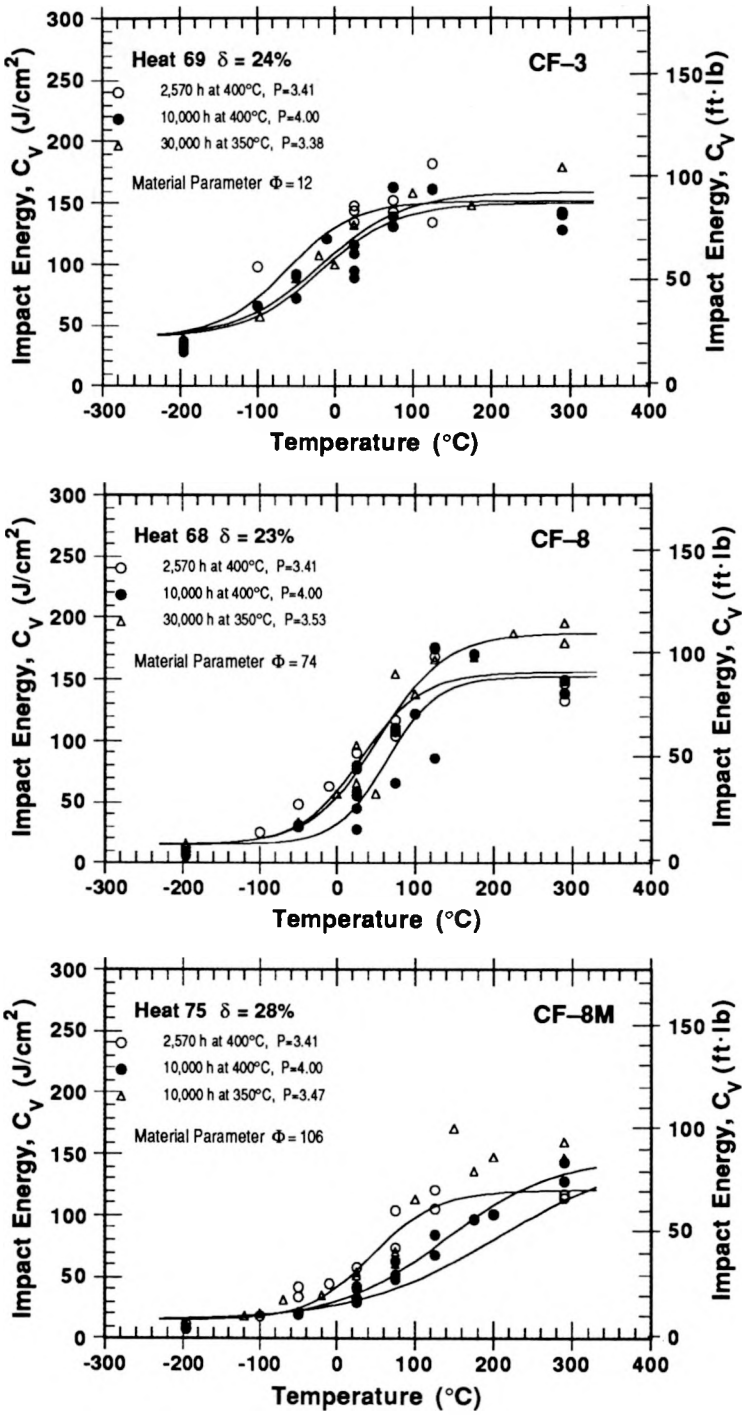

Figure 13. Charpy transition curves for CF–3, CF–8, and CF–8M steels aged to P values between 3.4 and 4.0

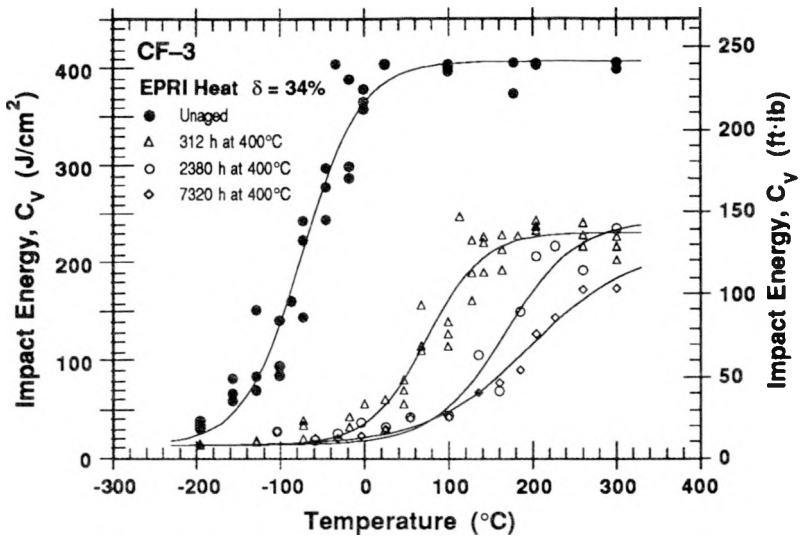

Figure 14. Charpy transition curves for CF–3 cast stainless steel aged at 400°C for various times. Charpy–impact data from Ref. 20.

long-term aging. The transition curves for Heat 68 ($\Phi \approx 74$) are also comparable but may not represent saturation. Because the minimum room-temperature impact energy is close to the lower-shelf energy, an increase in CTT would decrease the impact energy at reactor temperatures without significantly changing room-temperature impact energy. The results for Heat 75 ($\Phi \approx 106$) do not indicate a saturation effect on the transition curve. Thus, although the room-temperature impact energy does not change for P values >3.5, the impact energy at reactor temperatures may continue to decrease with time. This behavior is not unique to CF–8M steels and was observed in the EPRI study[20] on CF–3 steel ($\Phi \approx 68$), as shown in Fig. 14. Long-term aging data are needed to establish the impact energies at reactor temperatures and to confirm whether a saturation effect in transition curves is achieved for some of the heats, e.g., heats with low values of material parameter Φ.

The Charpy data for Heats 68, 69, and 75 also indicate that the transition curves for 350°C aging are lower than those after aging for an equivalent time at 400°C, particularly for the CF–8M steel. The mid-shelf CTT for the three grades of cast stainless steel aged up to 30,000 h at 320, 350, 400, and 450°C are plotted as a function of the aging parameter P in Fig. 15. The increase in CTT (i.e., slope of the solid lines) for CF–8M steels is graeter by a factor of two than that for CF–3 or CF–8 steels. For all heats, the values of CTT for 400 or 450°C aging are lower than those after aging at lower temperatures for equivalent times, i.e., for the same values of P. These results raise an important issue, i.e., the kinetics of embrittlement established from the room-temperature Charpy data are not representative of the changes in Charpy-impact energy at reactor temperatures. Also, the data for minimum Charpy-impact energy at 290°C show poor correlation with either the aging parameter P or the material parameter Φ.

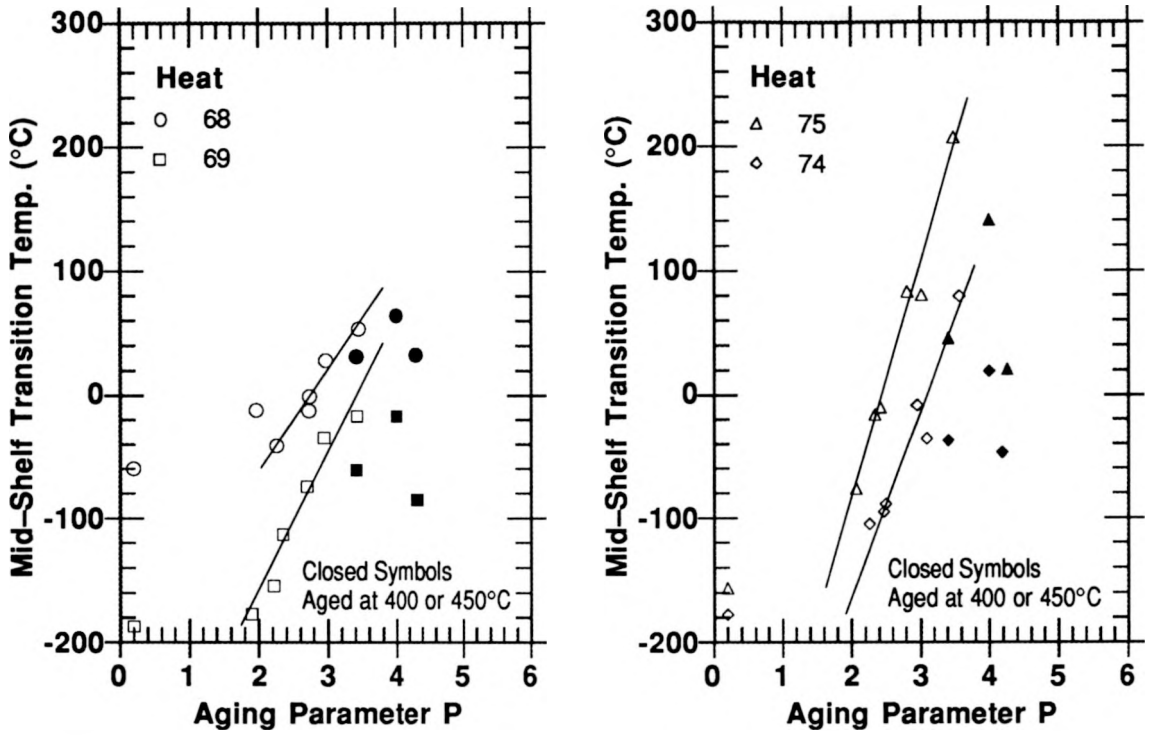

Figure 15. Change in mid-shelf CTT with thermal aging for CF-8 (Heat 68), CF-3 (Heat 69), and CF-8M (Heats 74 and 75) cast stainless steel. The solid lines represent the change in CTT with P for aging temperatures ≤350°C.

3 Recovery Annealing

Microstructural and annealing studies[8,13-15] on laboratory- and reactor-aged materials have been conducted to investigate the possibility of recovering the mechanical properties of embrittled materials. The results indicate that the formation of α' phase by spinodal decomposition is the primary mechanism for embrittlement. The α' phase is not stable at temperatures >550°C. The mechanical properties can be recovered by annealing the embrittled cast stainless steels for 1 h at 550°C and water-quenching to dissolve the α' phase while avoiding the formation of σ phase. The influence of annealing on the Charpy transition curves for three laboratory-aged heats and service-aged material from the KRB reactor is shown in Figs. 16 and 17, respectively. The service-aged pump cover plate was obtained from the KRB reactor, which was in service in Gundremmingen, West Germany, for ≈12 y (i.e., ≈8 y, or ≈68,000 h, at a service temperature of 284°C). The chemical composition and ferrite content of the KRB material are shown in Table 1. The results indicate essentially complete recovery from embrittlement; the transition curves for the annealed materials agree well with those for the unaged steel. Microstructural examination of the annealed material showed no α' phase, but the size and distribution of the G phase were the same as in the aged material.[13-15]

Charpy data for laboratory-aged materials indicate that the kinetics of embrittlement can also be obtained from the reembrittlement of recovery-annealed material. The Charpy-

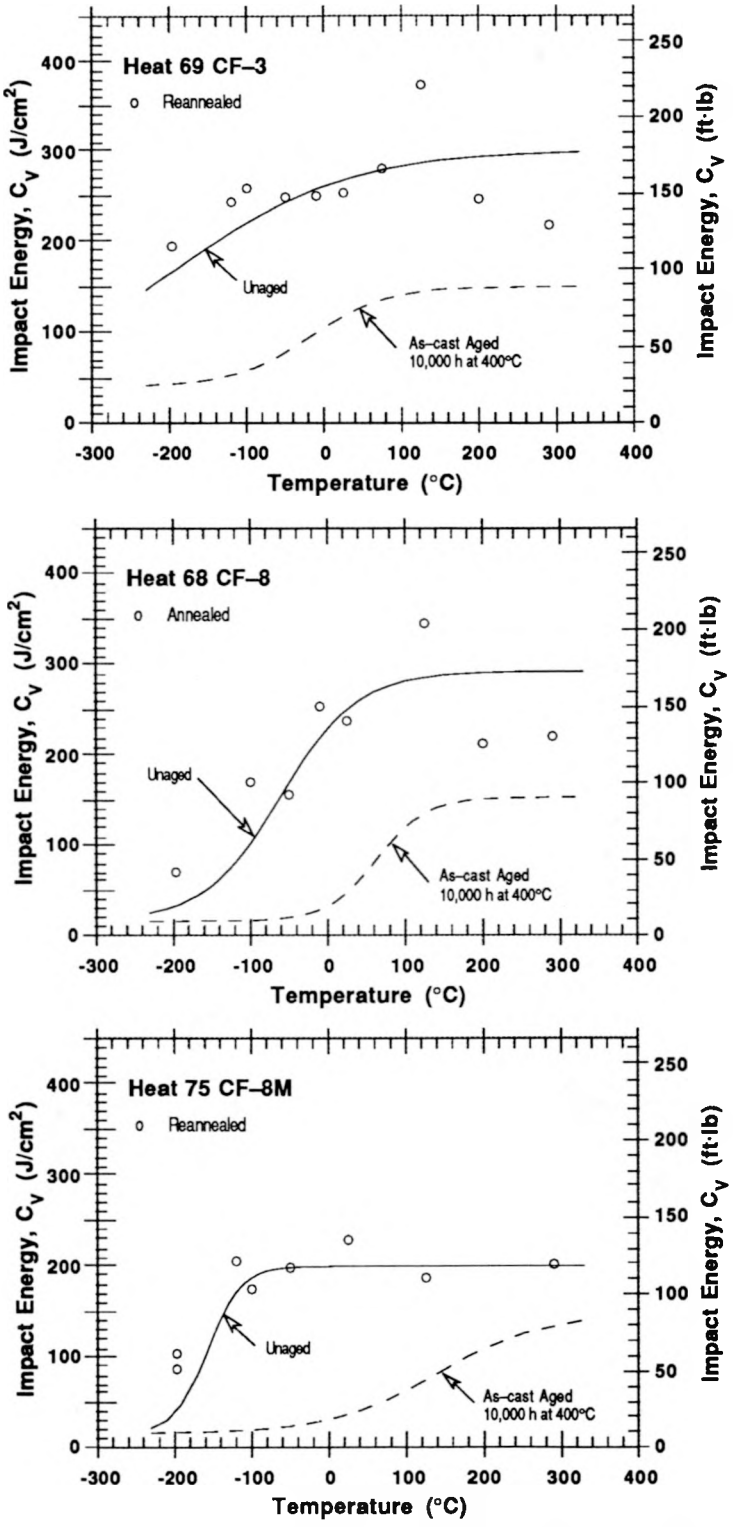

Figure 16. Effect of annealing on the Charpy transition curves for thermally aged CF–3, CF–8, and CF–8M steel. Embrittled materials shown by dashed lines.

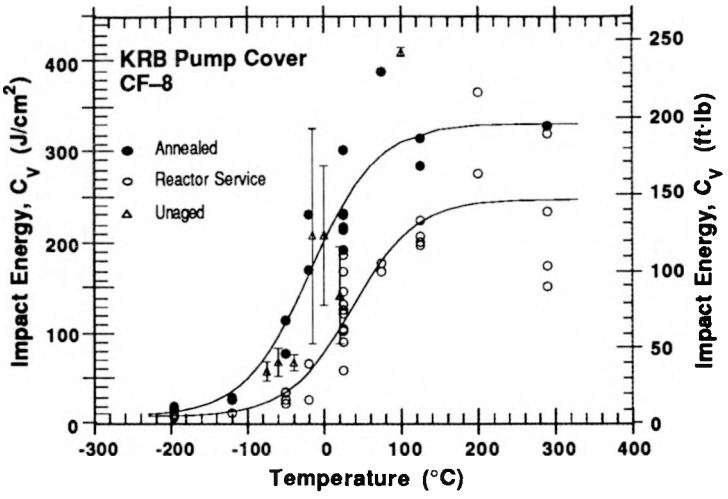

Figure 17. Effect of annealing on the Charpy transition curve for the KRB pump cover plate

impact data for recovery-annealed CF-3, CF-8, and CF-8M steels aged up to 10,000 h at 400, 350, and 320°C are given in Table 4. The Charpy transition data for the recovery-annealed materials aged for 10,000 h at 400°C are shown in Fig. 16. The transition curves are virtually the same as those for the as-cast material aged for 10,000 h at 400°C. The aging behaviors of as-cast and recovery-annealed steels are shown in Fig. 18. The activation energies of the as-cast materials are 168±37, 167±48, and 146±21 kJ/mole for Heats 68, 69, and 75, respectively. The Charpy data for recovery-annealed and aged Heats 68, 69, and 75, respectively, yield activation energies of 122±41, 176±49, and 130±28 kJ/mole, i.e., the kinetics of re-embrittlement of Heat 69 are comparable and those of Heats 68 and 75

Table 4. Charpy-impact test results for recovery-annealed and aged cast stainless steel

Specimen Number[a]	Heat	Aging Temp. (°C)	Aging Time (h)	Test Temp. (°C)	Impact Energy (J/cm^2)	Yield Load (kN)	Max. Load (kN)
			CF-8 Grade				
683-55A	68	–	–	-197	70.0	15.838	19.607
683-54A	68	–	–	-50	155.3	12.977	20.994
683-53A	68	–	–	25	237.4	10.946	16.785
683-52A	68	–	–	125	345.0	9.267	14.451
683-51A	68	–	–	290	220.5	7.382	11.883
684-52A	68	–	–	-100	169.6	14.276	21.472
684-53A	68	–	–	-10	253.3	11.893	18.572
684-54A	68	–	–	200	212.7	8.144	12.850
68-317A	68	320	3,000	25	214.5	10.770	16.024
68-318A	68	320	3,000	25	184.3	10.926	17.322
68-319A	68	320	10,000	25	157.3	12.010	18.455
68-320A	68	320	10,000	25	208.0	11.893	18.211
68-308A	68	350	100	25	236.1	11.327	17.683
68-309A	68	350	300	25	230.9	11.112	17.020
68-310A	68	350	300	25	280.8	11.883	17.615
68-311A	68	350	1,000	25	160.8	10.946	17.273

Table 4. (Contd.)

Specimen Number[a]	Heat	Aging Temp. (°C)	Aging Time (h)	Test Temp. (°C)	Impact Energy (J/cm^2)	Yield Load (kN)	Max. Load (kN)
68-312A	68	350	1,000	25	166.4	10.809	17.527
68-313A	68	350	3,000	25	84.1	11.063	14.578
68-314A	68	350	3,000	25	65.6	11.239	14.061
68-315A	68	350	10,000	25	55.2	12.782	15.008
68-316A	68	350	10,000	25	71.1	12.352	16.063
684-58A	68	400	50	25	213.7	11.278	16.941
684-59A	68	400	50	25	179.0	11.249	16.600
68-301A	68	400	100	25	211.5	12.059	17.683
684-60A	68	400	100	25	186.0	11.756	17.635
68-302A	68	400	300	25	175.9	12.352	18.611
68-303A	68	400	300	25	199.7	11.835	18.347
68-304A	68	400	1,000	25	126.5	11.903	17.254
68-305A	68	400	1,000	25	103.9	12.791	16.287
68-306A	68	400	3,000	25	73.7	11.678	14.803
68-307A	68	400	3,000	25	78.5	11.962	14.783
683-56A	68	400	10,000	-197	12.1	13.358	13.358
684-55A	68	400	10,000	-120	28.0	16.277	16.277
683-57A	68	400	10,000	-50	32.3	14.051	14.325
681-59A	68	400	10,000	25	82.6	13.368	16.063
682-59A	68	400	10,000	25	66.7	12.811	15.164
683-58A	68	400	10,000	75	82.2	10.800	15.076
683-59A	68	400	10,000	290	129.8	7.597	12.284
				CF-3 Grade			
693-55A	69	-	-	-197	194.1	11.249	25.251
693-54A	69	-	-	-50	248.4	11.200	20.789
693-53A	69	-	-	25	253.5	9.833	17.283
693-52A	69	-	-	125	373.5	7.636	13.612
693-51A	69	-	-	290	218.1	6.308	11.239
694-51A	69	-	-	-120	242.7	10.966	23.474
694-52A	69	-	-	-100	258.5	11.219	22.800
694-53A	69	-	-	-10	249.9	10.780	18.865
694-54A	69	-	-	75	280.3	8.886	14.588
694-55A	69	-	-	200	246.6	7.187	12.323
69-305A	69	320	1,000	25	244.7	9.999	17.088
69-306A	69	320	1,000	25	270.7	10.223	17.391
69-307A	69	320	3,000	25	271.8	10.175	17.469
69-308A	69	320	3,000	25	258.2	10.487	17.723
69-309A	69	320	10,000	25	289.4	11.132	18.699
69-310A	69	320	10,000	25	231.5	10.741	18.015
69-318A	69	350	100	25	261.8	10.516	17.498
692-56A	69	350	100	25	235.3	10.145	16.688
69-319A	69	350	300	25	248.2	10.175	17.186
692-57A	69	350	300	25	234.3	10.194	17.879
69-301A	69	350	1,000	25	212.2	10.487	17.996
692-59A	69	350	1,000	25	219.2	10.380	17.332
69-320A	69	350	3,000	25	229.0	10.477	18.230
692-58A	69	350	3,000	25	203.8	10.272	17.225
69-303A	69	350	10,000	25	143.4	10.780	17.723
69-311A	69	400	50	25	232.2	10.136	17.459
691-56A	69	400	50	25	228.2	10.526	17.361
69-314A	69	400	100	25	236.5	10.438	18.133
691-59A	69	400	100	25	230.6	10.946	18.035
69-312A	69	400	300	25	248.9	10.682	18.523

Table 4. (Contd.)

Specimen Number[a]	Heat	Aging Temp. (°C)	Aging Time (h)	Test Temp. (°C)	Impact Energy (J/cm^2)	Yield Load (kN)	Max. Load (kN)
691-57A	69	400	300	25	180.2	10.751	17.625
69-313A	69	400	1,000	25	167.8	10.946	18.338
691-58A	69	400	1,000	25	129.9	10.839	17.273
69-316A	69	400	3,000	25	138.5	10.555	17.410
691-60A	69	400	3,000	25	155.3	11.464	17.459
691-54A	69	400	10,000	-197	39.3	12.831	17.498
692-51A	69	400	10,000	-120	118.5	11.171	19.343
691-55A	69	400	10,000	-50	109.9	13.690	19.900
693-60A	69	400	10,000	25	103.7	11.571	17.635
694-60A	69	400	10,000	25	130.2	11.874	17.508
692-52A	69	400	10,000	75	161.9	8.095	14.364
692-53A	69	400	10,000	290	129.6	7.528	12.635
			CF-8M Grade				
754-57A	75	-	-	-197	86.6	18.142	24.128
753-60A	75	-	-	-50	198.0	13.631	21.003
753-59A	75	-	-	25	228.3	12.264	18.865
753-58A	75	-	-	125	186.7	10.116	15.770
753-57A	75	-	-	290	201.5	8.134	13.524
754-60A	75	-	-	-197	103.8	18.601	25.300
754-58A	75	-	-	-120	205.2	16.717	25.192
754-59A	75	-	-	-100	174.8	16.453	24.987
754-52A	75	320	3,000	25	184.8	12.821	18.953
754-53A	75	320	3,000	25	209.2	12.411	18.709
754-54A	75	320	10,000	25	185.4	13.153	19.832
754-55A	75	320	10,000	25	170	14.041	18.738
752-59A	75	350	300	25	234.1	13.133	19.822
752-60A	75	350	300	25	244.8	13.084	20.007
753-51A	75	350	1,000	25	182.8	13.182	19.675
753-52A	75	350	1,000	25	180.6	13.172	19.226
753-53A	75	350	3,000	25	115.9	13.426	18.416
753-54A	75	350	3,000	25	122.8	13.270	19.343
753-55A	75	350	10,000	25	82.4	14.705	19.500
754-51A	75	350	10,000	25	33.7	15.467	15.789
751-56A	75	400	100	25	227.0	13.250	20.525
751-57A	75	400	100	25	223.9	12.801	19.666
751-58A	75	400	300	25	208.0	13.573	20.955
751-59A	75	400	300	25	189.8	13.553	20.369
751-60A	75	400	1,000	25	86.2	13.553	17.683
752-56A	75	400	1,000	25	68.3	13.700	16.502
752-57A	75	400	3,000	25	57.3	13.827	16.756
752-58A	75	400	3,000	25	70.0	13.963	17.098
75-301A	75	400	10,000	-197	9.1	15.330	15.330
75-302A	75	400	10,000	-50	30.7	16.277	16.277
75-365A	75	400	10,000	25	43.4	14.871	16.531
75-366A	75	400	10,000	25	37.7	15.330	16.980
75-303A	75	400	10,000	75	62.4	13.211	16.404
75-304A	75	400	10,000	290	95.4	9.970	14.334

[a] All specimens aged 10,000 h at 400°C and annealed for 1 h at 550°C and water quenched prior to aging.

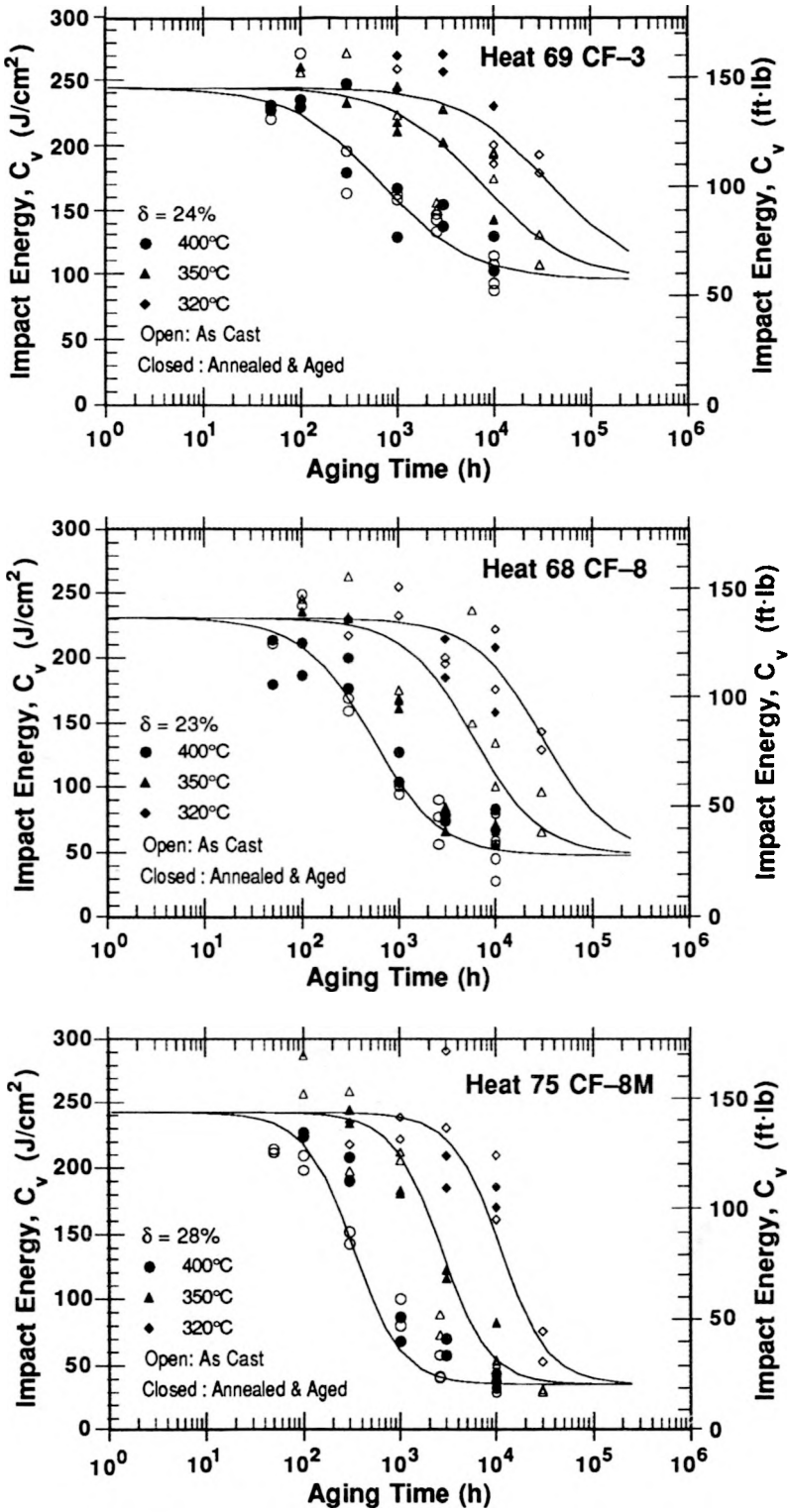

Figure 18. Effect of thermal aging on room-temperature impact energy of unaged and recovery-annealed CF-3, CF-8, and CF-8M steel. The solid lines represent the aging behavior of the as-cast materials.

are slightly faster than the kinetics of embrittlement of the as-cast materials. However, there is significant overlap in the 95% confidence limits between the values obtained for as-cast and recovery-annealed materials. The difference in the kinetics of Heats 68 and 75 is primarily due to the aging behavior at 400°C. The decrease in impact energy at 320°C is comparable for as-cast and recovery-annealed materials.

The results indicate that baseline mechanical properties and possibly the kinetics of embrittlement of cast stainless steels can be determined from the recovery-annealed material. This may be very useful for evaluating degradation of mechanical properties of service-aged components, where the baseline mechanical properties or archive material are generally not available.

4 Conclusions

Charpy-impact data are presented for several experimental and commercial heats of cast stainless steel that were aged up to 30,000 h at temperatures of 290-450°C. The results indicate that, for a specific cast stainless steel, the extent of embrittlement, i.e., the minimum room-temperature impact energy that would be achieved after long-term aging, depends on the chemical composition and ferrite morphology of the steel. A correlation is presented for estimating the extent of embrittlement from known material information.

The results indicate that the extent and rate of embrittlement depend on material parameters, i.e., ferrite morphology and chemical composition of the steel. Ferrite morphology strongly affects the extent of embrittlement, whereas material composition influences the kinetics of embrittlement. Small changes in the constituent elements of the cast material can cause the kinetics of embrittlement to vary significantly.

Annealing studies indicate that the degradation in mechanical properties due to thermal embrittlement can be reversed by annealing the embrittled material for 1 h at 550°C and then water quenching. The kinetics of embrittlement can also be obtained from aging studies on the reembrittlement of recovery-annealed material. This procedure may be useful for establishing the baseline mechanical properties and kinetics of embrittlement of service-aged components.

Acknowledgments

This work was supported by the Office of Nuclear Regulatory Research of the U.S. Nuclear Regulatory Commission. The authors are grateful to A. Sather, T. M. Galvin, L. Y. Bush, G. M. Dragel, and W. F. Burke for their contribution to the experimental effort. The authors also thank J. Muscara, W. J. Shack, and T. F. Kassner for their helpful discussions.

References

1. A Trautwein and W. Gysel, *Influence of Long Time Aging of CF-8 and CF-8M Cast Steel at Temperatures Between 300 and 500°C on the Impact Toughness and the Structure*

Properties, in Stainless Steel Castings, V. G. Behal and A. S. Melilli, eds., ASTM STP 756, Philadelphia, PA, pp. 165–189 (1982).

2. O. K. Chopra and H. M. Chung, *Long-Term Embrittlement of Cast Duplex Stainless Steels in LWR Systems: Annual Report, October 1983–September 1984*, NUREG/CR–4204, ANL–85–20 (March 1985); *Nucl. Eng. Des.* **89**, 305 (1985).

3. O. K. Chopra and H. M. Chung, *Long-Term Embrittlement of Cast Duplex Stainless Steels in LWR Systems: Annual Report, October 1984–September 1985*, NUREG/CR–4503, ANL–86–3 (Jan. 1986).

4. O. K. Chopra and H. M. Chung, *Long-Term Embrittlement of Cast Duplex Stainless Steels in LWR Systems: Semiannual Report, October 1985–March 1986*, NUREG/CR–4744 Vol. I, No. 1, ANL–86–54 (Sept. 1986).

5. O. K. Chopra and G. Ayrault, *Long-Term Embrittlement of Cast Duplex Stainless Steels in LWR Systems:*, in Materials Science and Technology Division Light-Water-Reactor Safety Research Program: Quarterly Progress Report, October–December 1983, NUREG/CR–3689 Vol. IV, ANL–83–85 Vol. IV, pp. 129–151 (Aug. 1984).

6. O. K. Chopra and H. M. Chung, *Long-Term Embrittlement of Cast Duplex Stainless Steels in LWR Systems:*, in Materials Science and Technology Division Light-Water-Reactor Safety Materials Engineering Research Programs: Quarterly Progress Report, January–March 1984, NUREG/CR–3998 Vol. I, ANL–84–60 Vol. I, p. 52 (Sept. 1984).

7. O. K. Chopra and H. M. Chung, *Aging Degradation of Cast Stainless Steels: Effects on Mechanical Properties*, in Environmental Degradation of Materials in Nuclear Power Systems–Water Reactors, G. J. Theus and J. R. Weeks, eds., The Metall. Soc., Warrendale, PA., pp. 737–748 (1988).

8. O. K. Chopra and H. M. Chung, *Effect of Low-Temperature Aging on the Mechanical Properties of Cast Stainless Steels*, in Properties of Stainless Steels in Elevated Temperature Service, M. Prager, ed., MPC–Vol. 26, PVP–Vol. 132, ASME, New York, pp. 79–105 (1988).

9. O. K. Chopra and H. M. Chung, *Long-Term Embrittlement of Cast Duplex Stainless Steels in LWR Systems: Semiannual Report, April–September 1987*, NUREG/CR–4744 Vol. 2, No. 2, ANL–89/6 (July 1989).

10. O. K. Chopra and H. M. Chung, *Long-Term Embrittlement of Cast Duplex Stainless Steels in LWR Systems: Semiannual Report, October 1987–March 1988*, NUREG/CR–4744 Vol. 3, No. 1, ANL–89/22 (Feb. 1990).

11. O. K. Chopra and H. M. Chung, *Long-Term Embrittlement of Cast Duplex Stainless Steels in LWR Systems: Semiannual Report, April–September 1988*, NUREG/CR–4744 Vol. 3, No. 2, ANL–90/5 (August 1990).

12. O. K. Chopra and A. Sather, *Initial Assessment of the Mechanisms and Significance of Low-Temperature Embrittlement of Cast Stainless Steels in LWR Systems*, NUREG/CR-5385, ANL-89/17 (Aug. 1990).

13. H. M. Chung and O. K. Chopra, *Microstucture of Cast Duplex Stainless Steel after Long-Term Aging*, in Proc. Second Int. Symp. on Environmental Degradation of Materials in Nuclear Power Systems - Water Reactors, Am. Nucl. Soc., LaGrange Park, IL, pp. 287-292 (1986).

14. H. M. Chung and O. K. Chopra, *Kinetics and Mechanism of Thermal Aging Embrittlement of Duplex Stainless Steels*, in Environmental Degradation of Materials in Nuclear Power Systems-Water Reactors, G. J. Theus and J. R. Weeks, eds., The Metall. Soc., Warrendale, PA, pp. 359-370 (1988).

15. H. M. Chung and O. K. Chopra, *Long-Term Aging Embrittlement of Cast Austenitic Stainless Steels - Mechanism and Kinetics*, in Properties of Stainless Steels in Elevated Temperature Service, M. Prager, ed., MPC-Vol. 26, PVP-Vol. 132, ASME, New York, pp. 17-34 (1988).

16. S. Bonnet, J. Bourgoin, J. Champredonde, D. Guttmann, and M. Guttmann, *Relationship between Evolution of Mechanical Properties of Various Cast Duplex Stainless Steels and Metallurgical and Aging Parameters: An Outline of Current EDF Programmes*, Mater. Sci. Technol. **6**, 221-229 (1990).

17. G. Slama, P. Petrequin, and T. Magep, *Effect of Aging on Mechanical Properties of Austenitic Stainless Steel Castings and Welds*, presented at SMIRT Post-Conference Seminar 6, Assuring Structural Integrity of Steel Reactor Pressure Boundary Components, Aug. 29-30, 1983, Monterey, CA.

18. Y. Meyzaud, P. Ould, P. Balladon, M. Bethmont, and P. Soulat, *Tearing Resistance of Aged Cast Austenitic Stainless Steel*, presented at Intl. Conf. on Thermal Reactor Safety (NUCSAFE 88), Oct. 1988, Avignon, France.

19. P. H. Pumphrey and K. N. Akhurst, *Aging Kinetics of CF3 Cast Stainless Steel in Temperature Range 300°C-400°C*, Mater. Sci. Technol. **6**, 211-219 (1990).

20. P. McConnell and J. W. Sheckherd, *Fracture Toughness Characterization of Thermally Embrittled Cast Duplex Stainless Steel*, Report NP-5439, Electric Power Research Institute, Palo Alto, CA (Sept. 1987).

Distribution for NUREG/CR-4744 Vol. 4, No. 1 (ANL-90/44)

Internal:

O. K. Chopra (25)
H. M. Chung (15)
C. Malefyt
W. J. Shack
C. E. Till
R. W. Weeks
TIS Files (3)
ANL Patent File
ANL Contract File

External:

NRC, for distribution per R5
ANL Libraries (2)
Manager, Chicago Operations Office, DOE
Materials and Components Technology Division Review Committee
H. Berger, Industrial Quality, Inc., Gaithersburg, MD
M. S. Dresselhaus, Massachusetts Institute of Technology, Cambridge, MA
S. J. Green, Electric Power Research Institute, Palo Alto, CA
R. A. Greenkorn, Purdue U., West Lafayette, IN
C.-Y. Li, Cornell U., Ithaca, NY
P. G. Shewmon, Ohio State U., Columbus
R. E. Smith, Electric Power Research Institute, NDE Ctr., Charlotte, NC
D. Atteridge, Battelle Pacific Northwest Laboratory
W. H. Bamford, Westinghouse Electric Corp., Pittsburgh
N. G. Cofie, Nutech, San Jose, CA
A. Cowan, Risley Nuclear Power Development Labs., Risley, Warrington, UK
E. L. Creamer, Shell Oil Co., Houston
W. H. Cullen, Materials Engineering Associates, Inc., Lanham, MD
B. J. L. Darlaston, Berkeley Nuclear Laboratories, Berkeley, Gloucestershire, UK
H. Domian, Alliance Research Center, Babcock & Wilcox Co., Alliance, OH
J. Gilman, Electric Power Research Inst., Palo Alto, CA
M. Guttmann, Electricité de France, Les Renardieres Roule de Sens, France
W. Gysel, Georg Fischer, Ltd., Schaffhausen, Switzerland
G. E. Hale, The Welding Institute, Abington, Cambridge, UK
P. Hedgecock, APTECH Engineering Services, Inc., Palo Alto, CA
B. Hemsworth, HM Nuclear Installations Inspectorate, London
C. G. Interrante, Center for Materials Science, National Institute of Standards and Technology, Gaithersburg, MD
J. Jansky, Buro für Technische Beratung, Leonberg, Germany
C. E. Jaske, CC Technologies, Cortest, Columbus, OH
D. de G. Jones, Matls. Sci. Div., Atomic Energy Corp., Pretoria, South Africa
C. Kim, Westinghouse Electric Corp., Pittsburgh
P. M. Lang, Office of Converter Reactor Deployment, U.S. Dept. of Energy, Washington, DC
G. J. Licina, Structural Integrity Associates, San Jose, CA
T. R. Mager, Westinghouse Electric Corp., Pittsburgh
Y. Meyzaud, Framatome, Paris
M. Prager, Materials Properties Council, Inc., New York

P. H. Pumphrey, National Power, Technology and Environment Center, Leatherhead, Surrey, UK
V. N. Shah, EG&G Idaho, Inc., P. O. Box 1625, Idaho Falls, Idaho
V. K. Sikka, Oak Ridge National Laboratory
G. Slama, Framatome, Paris La Defense, France
G. D. W. Smith, Oxford University, Oxford, UK
H. D. Solomon, General Electric Co., Schenectady, NY
D. M. Stevens, Lynchburg Research Center, Babcock & Wilcox Co., Lynchburg, VA
L. Taylor, Nuclear Electric plc., Chelsford Rd., Knutsford, Cheshire, UK
J. M. Vitek, Oak Ridge National Laboratory
J. Wilks, AMOCO, P. O. Box 3011, Naperville, IL

NRC FORM 335 (2–89) NRCM 1102, 3201, 3202

U. S. NUCLEAR REGULATORY COMMISSION

BIBLIOGRAPHIC DATA SHEET

(See instructions on the reverse)

1. REPORT NUMBER *(Assigned by NRC. Add Vol., Supp., Rev., and Addendum Numbers, if any.)*

NUREG/CR–4744
Vol. 4, No. 1
ANL–90/44

2. TITLE AND SUBTITLE

Long–Term Embrittlement of Cast Duplex Stainless Steels in LWR Systems

Semiannual Report
October 1988–March 1989

3. DATE REPORT PUBLISHED

MONTH	YEAR
May	1991

4. FIN OR GRANT NUMBER

A2243

5. AUTHOR(S)

O. K. Chopra, H. M. Chung

6. TYPE OF REPORT

Technical; Semiannual

7. PERIOD COVERED *(Inclusive Dates)*

October 1988–March 1989

8. PERFORMING ORGANIZATION – NAME AND ADDRESS *(If NRC, provide Division, Office or Region, U.S. Nuclear Regulatory Commission, and mailing address; if contractor, provide name and mailing address.)*

Argonne National Laboratory
9700 South Cass Avenue
Argonne, IL 60439

9. SPONSORING ORGANIZATION – NAME AND ADDRESS *(If NRC, type "Same as above": if contractor, provide NRC Division, Office or Region, U.S. Nuclear Regulatory Commission, and mailing address.)*

Division of Engineering
Office of Nuclear Regulatory Research
U. S. Nuclear Regulatory Commission
Washington, DC 20555

10. SUPPLEMENTARY NOTES

11. ABSTRACT (200 words or less)

This progress report summarizes work performed by Argonne National Laboratory on long–term embrittlement of cast duplex stainless steels in LWR systems during the six months from October 1988 to March 1989. Charpy–impact data are presented for several heats of cast stainless steel aged at temperatures between 320 and 450°C for times up to 30,000 h. Thermal aging decreases impact energy and shifts transition curves to higher temperatures. A saturation effect is observed for room–temperature impact energy and upper–shelf energy. Charpy data are analyzed to obtain the activation energy of the kinetics of embrittlement. The results suggest that the activation energy of embrittlement is not constant in the temperature range of 290–400°C, but increases as temperature decreases. A correlation is presented for estimating the extent of embrittlement of cast stainless steels from known material parameters. The degradation in mechanical properties can be reversed by annealing the embrittled material for 1 h at 550°C and then water quenching.

12. KEY WORDS/DESCRIPTORS *(List words or phrases that will assist researchers in locating this report.)*

Cast duplex stainless steel
Thermal aging
Ferrite spinodal decomposition
Embrittlement
Fracture toughness
Impact strength

13. AVAILABILITY STATEMENT

Unlimited

14. SECURITY CLASSIFICATION

(This Page)

Unclassified

(This Report)

Unclassified

15. NUMBER OF PAGES

16. PRICE

NRC FORM 335 (2–89)